LIGHT GENERATION AND MANIPULATION FROM NONLINEAR RANDOMLY DISTRIBUTED DOMAINS IN SBN

CAN YAO

ICFO – INSTITUT DE CIÈNCIES FOTÒNIQUES

UNIVERSITAT POLITÈCNICA DE CATALUNYA

BARCELONA, 2014

LIGHT GENERATION AND MANIPULATION FROM NONLINEAR RANDOMLY DISTRIBUTED DOMAINS IN SBN

CAN YAO

under the supervision of

PROFESSOR JORDI MARTORELL

&

DOCTOR FRANCISCO RODRÍGUEZ

submitted this thesis in partial fulfillment

of the requirements for the degree of

DOCTOR

by the

UNIVERSITAT POLITÉCNICA DE CATALUNYA

BARCELONA, 2014

Dedicated to my loving family

Acknowledgments

First and foremost, I want to express my sincere gratitude to Prof. Dr. Jordi Martorell, my supervisor of this PhD thesis, for providing me the opportunity to work on the project "Generation of light in random structures", guiding and motivating me all through the work of this thesis. With his immense experience and knowledge, meticulous and rigorous scholarship, he has always been giving me valuable advice, and inspiring me to overcome all the challenges we ever met.

Deepest gratitude is also due to Dr. Francisco Rodríguez, without whose knowledge and assistance this study would not have been successful. Dr. Francisco has accompanied me all through this project, and I have learnt a lot from him, both in knowledge and his strict attitude in science. I am greatly indebted to him.

I also give my sincere gratitude to Prof. Dr. Jorge Bravo-Abad for his valuable help in developing the theoretical models used in the thesis.

I would also like to take this opportunity to thank all the work members in ICFO-the institute of photonic sciences, whose valuable dedication to the administrative and instrumental services has provided me an

excellent environment to focus on my work. Besides, they have made my time here more pleasant and memorable. I thank ICFO for giving me so many opportunities to learn new stuffs beyond science, and I will benefit from the invaluable knowledge and skills in language, business, and communication in a very long term.

Special thanks go to all my past and present group members, Roberto, Luis, Marc, Sergio, Alberto, Marina, Luat, Xavi, Rafael, Pablo, Camila, Paola, David, and Francesco, and other ICFO colleagues, Johann, Tonglai Chen, Xiaojuan Shi, Na Lou, Xiaojie Yang, Chaitanya, Sotiris, Dhriti, Chirag, Giorgio, Armand, Marc, Ulrich, Naeimeh, Carmen, Luis Martinez, and many others, for the discussion in science, advice in experiment set-up, or sample processing, especially, their friendship and help in my life.

I also would like to thank Prof. Yuren Wang, my supervisor of the master thesis in photonic crystal in Chinese Academy of Science, who guided me the first step into the field of photonics, and he has been giving me invaluable advice not only in academy but also in my personal life.

I would like to express my deepest love to my dearest family. I thank my dearest husband, Dr. Xingxing Huang. For his continuous encouragement and absolute support, I am able to do the best that I can. I thank my dearest parents and parents in law, Baoxiang Ma, Zhenshan Yao, Pengzhen Yang and Jinrui Huang, for their forever confidence in

me. I also thank my dearest brother, Yan Yao, who has been taking good care of my family when I am studying abroad. Special thanks also go to my daughter Yueyao Huang, who has been a source of happiness and a huge motivation of fulfillment during my thesis writing.

Abstract

Disordered media with refractive index variations can be found in the atmosphere, the ocean, and in many materials or biological tissues. Several technologies that make use of such random media, as image formation, satellite communication, astronomy or microscopy, must deal with an unavoidable light scattering or diffusion. This is why for many years light propagation through random media has been a subject of intensive study. Interesting phenomena such as speckle, coherent backscattering or random lasing have been discovered and studied. More recently, researchers are beginning to investigate mechanisms to control light propagation through such media to enhance light transmission and sharpen the focus.

On the other hand, it has been known for several years that nonlinear random structures are able to generate light in an ultra-broad frequency range, without the need of angle or temperature tuning. Particularly interesting is the nonlinear light diffusion observed from materials with no change in the refractive index and which appear to be fully diffusion less to linear light propagation. However, a comprehensive understanding of the scattering when a nonlinear interaction takes place has not yet been given.

The core of the thesis focuses on the study of the nonlinear light generation and propagation from crystalline structures with disordered nonlinear domains but with a homogenous refractive index. A random distribution of non-linear domains is found naturally in the Strontium Barium Niobate (SBN) ferroelectric crystal. As opposed to other mono-domain nonlinear optical crystals commonly used for frequency up-conversion, such as Potassium Titanyl Phosphate (KTP) or Lithium Niobate ($LiNbO_3$), in SBN the nonlinear domain size is, typically, on the order of the coherence length or many times smaller than the size of the whole crystal. Such domains are usually several times longer in the c-axis direction relative to the plane perpendicular to that axis. Adjacent domains exhibit antiparallel polarization along such crystalline axis, with no change in refractive index.

In Chapter 1 we give a brief introduction to light generation and propagation in random media, describing the speckle, light manipulation and second harmonic generation (SHG).

In chapter 2, we study the nonlinear light generation and manipulation from a transparent SBN crystal. In its theoretical description we use a two-dimensional random structure consisting of a homogeneous background polarized in one direction with uniform rectangular boundaries, and a group of square reverse polarization domains with random sizes and located in random positions. The SHG from each domain is obtained using the Green´s function formalism. In the experiments, we alter the ferroelectric domain structure of the SBN crystal by electric field poling or thermal treatments at different

temperatures. The SBN crystal structures after such different treatments are shown to be characterized by their SHG patterns.

In chapter 3, by measuring the spatial distribution of the second harmonic light in the c-plane, we demonstrate that the randomness in the nonlinear susceptibility results in a speckle pattern. We explain the observations as a result of the linear interference among the second harmonic waves generated in all directions by each of the nonlinear domains.

In chapter 4, we report on our experimental implementation of the wave-front phase modulation method to control and focus the SHG speckle from the random SBN crystal. This research creates a bridge between light phase modulation and nonlinear optics. Finally we perform a theoretical analysis to demonstrate enhanced efficiencies for nonlinear light focusing by the wave-front phase modulation method in different directions. Various types of nonlinear structures are considered, including the homogeneous rectangular crystal, the group of random domains, and the combination of both.

Resumen

Los medios desordenados con índices de refracción variables se pueden encontrar en la atmósfera, el océano, en muchos materiales o tejidos biológicos. Varias tecnologías que hacen uso de dichos medios como la formación de imágenes, la comunicación vía satélite, la astronomía o la microscopía, deben afrontar la dispersión o difusión de la luz. Por este motivo la propagación de la luz a través de medios aleatorios ha sido investigada exhaustivamente desde hace muchos años. Se han descubierto y estudiado fenómenos como el moteado, la retrodispersión coherente o el láser aleatorio. Recientemente, se están empezando a investigar varios mecanismos que permiten controlar la propagación de la luz a través de tales medios para aumentar la transmisión y mejorar el enfoque de la luz.

Por otra parte, se conoce desde hace tiempo que las estructuras aleatorias no lineales son capaces de generar luz en un rango de frecuencia ultra-ancha, sin la necesidad de sintonización de ángulo o temperatura. Es interesante la difusión no lineal de luz observada en materiales que no cambian su índice de refracción y que no presentan difusión a la propagación lineal de la luz. Sin embargo, aún no se ha

dado una explicación completa de la dispersión que se produce cuando tiene lugar una interacción no lineal.

El núcleo de la tesis se centra en el estudio de la generación y la propagación de luz no lineal en estructuras cristalinas con dominios no lineales desordenados pero con un índice de refracción homogéneo. Una distribución aleatoria de dominios no lineales se puede encontrar en el cristal ferroeléctrico de estroncio-bario-niobato (SBN). A diferencia de otros cristales no lineales monodominio, de uso común para la conversión ascendente de frecuencia, tales como el fosfato de potasio titanil (KTP) o el niobato de litio ($LiNbO_3$), en el SBN el tamaño de dominio no lineal es típicamente del orden de la longitud de coherencia o más pequeño que el tamaño del cristal. Tales dominios son por lo general mucho más largos en la dirección del eje c en comparación con la dimensión en el plano perpendicular a ese eje. Dominios adyacentes exhiben polarización antiparalela a lo largo de dicho eje cristalino sin cambio en el índice de refracción.

En el capítulo 1 se proporciona una breve introducción a la generación y la propagación de la luz en medios aleatorios, describiendo los fenómenos de moteado, manipulación de la luz y generación de segundo armónico (SHG).

En el capítulo 2, se estudia la generación y la manipulación de luz no lineal a partir de un cristal transparente SBN. En su descripción teórica la SHG de cada dominio se obtiene usando el formalismo de la función de Green. En los experimentos, se altera la estructura del dominio ferroeléctrico del cristal SBN por polarización del campo eléctrico o

tratamiento térmico a diferentes temperaturas. Las estructuras cristalinas SBN después de tales tratamientos se caracterizan por sus patrones de SHG.

En el capítulo 3, mediante la medida de la distribución espacial del segundo armónico en el plano c, se demuestra que la aleatoriedad de la susceptibilidad no lineal resulta en un patrón moteado. Se explican teóricamente las observaciones presentadas como resultado de la interferencia lineal entre las ondas de segundo armónico generadas en todas las direcciones por cada uno de los dominios no lineales.

En el capítulo 4, se describe el montaje experimental planteado para controlar y enfocar el moteado SHG del cristal aleatorio SBN por medio del método de modulación de fase del frente de onda (MFFO). Finalmente se realiza un análisis teórico para aumentar las eficiencias del enfoque de luz no lineal en diferentes direcciones por el método MFFO. Se consideraron diversos tipos de estructuras no lineales como un cristal homogéneo rectangular, un grupo de dominios aleatorios y la combinación de ambos.

Publications

1. C. Yao, F. J. Rodríguez, J. Bravo-Abad, and J. Martorell, "Wave-front phase-modulation control and focusing of second-harmonic light generated in transparent nonlinear random structures," Physical Review A, vol. 87, no. 063804, Jun. 2013.

2. C. Yao, F. J. Rodriguez, and J. Martorell, "Controlling the diffused nonlinear light generated in random materials," Optics letters, vol. 37, no. 10, pp. 1676–1678, May 2012.

3. F. J. Rodríguez, C. Yao, J. L. Domínguez-Juárez, J. Bravo-Abad, and J. Martorell, "Observation of speckle pattern formation in transparent nonlinear random media," Optics letters, vol. 36, no. 8, pp. 1347–1349, Apr. 2011.

Contents

Chapter 1

Introduction

Light propagation in random structures has attracted much attention due to coherent effects such as random lasing, coherent backscattering and light localization. Generally speaking, the term ¨random structure¨ in the linear optics context, refers to structures with inhomogeneous refractive index distribution, such as powders or suspensions. However, in nonlinear optics, there are structures with a homogeneous refractive index but a disordered distribution of the nonlinear susceptibility. For example, some ferroelectric crystals, such as Strontium-Barium Niobate (SBN), are transparent for linear light propagation, whereas the anti-parallel polarization of its ferroelectric domains may be distributed randomly in the crystal. Thus, its nonlinear light generation presents effects from a disordered structure.

The goal of this thesis is to investigate the coherent effects in the nonlinear light generation in random structures. Additionally, inspired by recent works in the control of linear light scattering through random media, we implement a novel method to re-concentrate the scattered light generation in random nonlinear materials.

This chapter contains three sections. The first section provides a general introduction to linear light propagation and generation in random media. This includes single and multiple scattering. Some examples of physical effects that appear in such kind of media are mentioned: coherent backscattering, random lasing, and speckle patterns. The concept of focusing light through random media is also briefly explained. More details about that can be found in chapter 3. The second section introduces the physics of nonlinear light generation and, more specifically, second harmonic generation. A special emphasis is given to phase-matching effects since they will be important to understand the following section and most part of this thesis. In the third section, we introduce the effects of a random structure on the nonlinear light generation.

1.1 General introduction to light propagation and generation in random media

When a beam of light propagates in a non-absorbing medium with a disordered inhomogeneous refractive index, the incident energy may be

spread in all directions while the frequency of the incident beam remains unchanged. This phenomenon is called elastic scattering, and, the scattered field can be computed by solving Maxwell wave equations for the macroscopic electromagnetic field subject to the appropriate boundary conditions [1].

Single scattering and multiple scattering

Depending on the complexity of the random system, there are two kinds of light scattering limiting regimes, single scattering and multiple scattering. In random media with a small number of scatterers separated with sufficiently large distances, light scattering is best described with the single light scattering limit where the light scattered from each scatterer is not affected by the presence of the rest of scatterers. In that limit, the total light scattering from the random media at the far field can be described by the coherent sum of the fields scattered from each scatterer.

On the other hand, a multiple scattering theory is needed for random media with a large number of scatterers, occupying a large portion of the total volume. In this case, the light intensity received by each scatterer from the rest of the scatterers may be larger than the light intensity received from the incident field itself. The description of scattering effects from such media may become complicated but, many interesting optical phenomena originate from such type of scattering.

For example, coherent backscattering is an enhanced scattering in the backward direction due to the interference among multiple time reverse light scattering paths [2-9]. See Figure 1.1a, two input beams A_{in} and B_{in} are scattered back in the directions A_{out} and B_{out}, and coherent interference occurs, while one can be obtained from the other by time inversion, when the angle between A_{in} and B_{out}, or B_{in} and A_{out} is zero. Light localization may happen in a random structure with high density of scatters, where some photons are trapped in a single loop path [10]. In that event the scatterers would play the role of an optical cavity. When the scatters are embedded in a gain medium, random lasing can occur [11-19]. In a random laser, light is confined not by conventional mirrors but by random multiple scattering (See Figure1.1b).

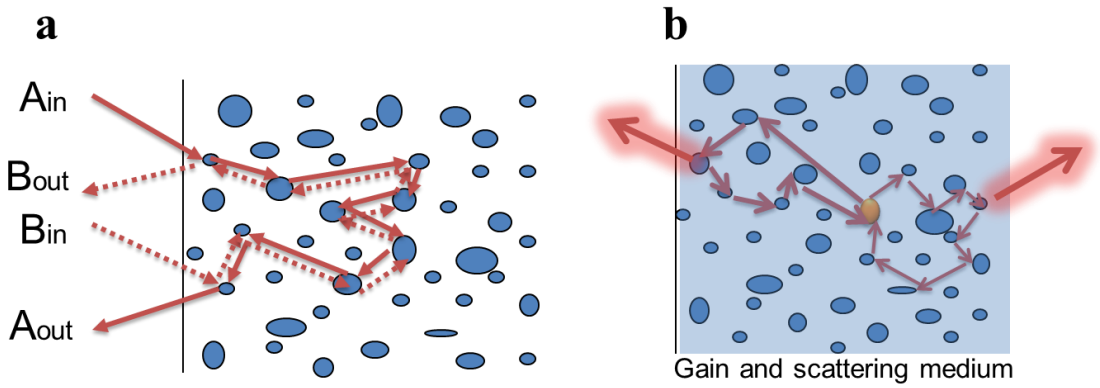

Figure 1.1: Schematic explanation of (a) coherent backscattering. (b) random lasing.

Speckle

When monochromatic and coherent light, such as laser light interacts with disordered media, the light is scattered into many different light paths with different propagation directions. The scattered light suffers constructive and destructive interferences forming an intensity pattern with bright and dark spots randomly distributed in space. This pattern is called the speckle. Some applications of the speckle effect have appeared in different fields since the invention of the laser [20-26]. Since it carries the material surface´s deformation information, it has been exploited, for instance, in holographic interferometry [27, 28]. On the other hand, speckle can be problematic in other applications such as, for example, in laser based display systems. In that event, reducing it becomes an important issue. Speckle reduction can be achieved by several means that produce many independent speckle patterns that are later averaged out on the detector [29, 30].

Control of linear light propagation in random medium

Interestingly, if the beam incident on the random medium is not a plane wave of light, but some structured beam with modulated phases on its cross-section, there is a special situation when the light will interfere

constructively at one single point after the random media, while the intensity vanishes at other points. In this case, the speckle disappears and one obtains a sharply focused beam. The principle of light focusing after random media is attributed to the time reversal symmetry (See Figure 1.2), which can be realized by the phase conjugation method. The phase conjugation can be obtained with different techniques, such as phase conjugation mirrors based on nonlinear effects, transmission matrix measurement and subsequent wave-front shaping by a spatial light modulator, or wave-front shape optimization using a feedback algorithm, etc. [31-35]. Furthermore, without the need of any lens, researchers have achieved sharp focusing beyond the diffraction limit under these operations [35, 36].

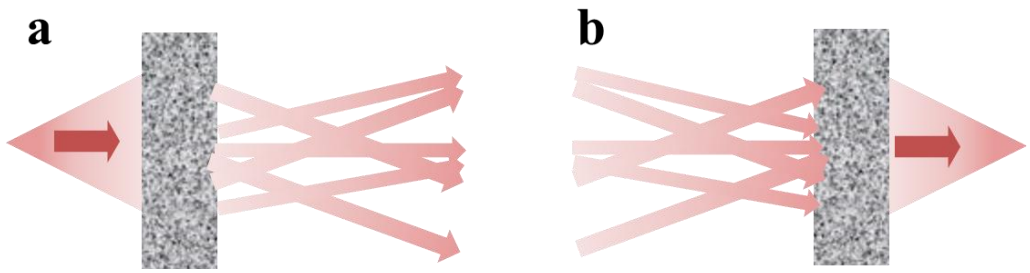

Figure 1.2: Schematic of (a) light scattering through a diffusive material and (b) light focused after one diffusive material under a wave-front shaped incident beam.

1.2 Nonlinear light propagation and second harmonic generation

Nonlinear light generation description

Light matter interaction can be described by using the relation between the electric field of light ***E(t)*** and the polarization ***P(t)*** of the material. In linear optics, the polarization induced in the material depends linearly on the electric field of light, and ***E(t)*** and ***P(t)*** have the linear relation:

$$\boldsymbol{P}(\boldsymbol{t}) = \varepsilon_0 \chi^{(1)} \boldsymbol{E}(\boldsymbol{t}) \tag{1.1}$$

where ε_0 is the electric permittivity of free space, and the constant $\chi^{(1)}$ is the linear susceptibility of the material.

In nonlinear optics, the optical response can be described by expanding ***P(t)*** into a power series of ***E(t)*** [37]:

$$\boldsymbol{P}(\boldsymbol{t}) = \varepsilon_0\left(\chi^{(1)}\boldsymbol{E}(\boldsymbol{t}) + \chi^{(2)}\boldsymbol{E}(\boldsymbol{t})^2 + \chi^{(3)}\boldsymbol{E}(\boldsymbol{t})^3 + \cdots\right) \equiv \boldsymbol{P}^{(1)}(\boldsymbol{t}) + \boldsymbol{P}^{(2)}(\boldsymbol{t}) + \boldsymbol{P}^{(3)}(\boldsymbol{t}) + \cdots \tag{1.2}$$

$\chi^{(2)}$ and $\chi^{(3)}$ are known as the second and the third order nonlinear susceptibilities of the material. $\chi^{(2)}$ is a third-rank tensor and $\chi^{(3)}$ is a fourth-rank tensor. Due to the fact that in centro-symmetric materials, the nonlinear susceptibilities remain unchanged under symmetry operations, all the even-order susceptibilities such as $\chi^{(2)}$ and $\chi^{(4)}$ etc., are 0 for all such materials. Many of the ferroelectric crystals are non-centro-symmetric at room temperature, so they may produce effective even-order nonlinear effects.

Second harmonic generation (SHG)

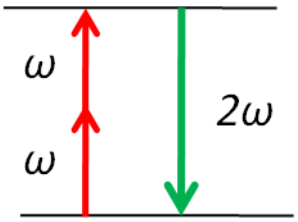

Figure 1.3: Energy diagram of second harmonic generation.

SHG is one of the most studied and used for applications second-order nonlinear optical process, where the power of the incident field at frequency ω is partially transferred into an oscillation at double frequency 2ω (See Figure 1.3) [38]. The polarization oscillating at 2ω acts as a source of electromagnetic dipole radiation. Due to the

dispersion in the refractive index, the fundamental wave travels at different phase velocity relative to the SH wave. Thus, the generated second harmonic waves at different locations in the nonlinear material can interfere constructively or destructively. Their sum increases due to their constructive interference up to the coherence length L_c, at which distance the polarization and the generated second harmonic waves come out of phase, and the total SHG begins to decrease due to the destructive interference (See Figure 1.4 a).

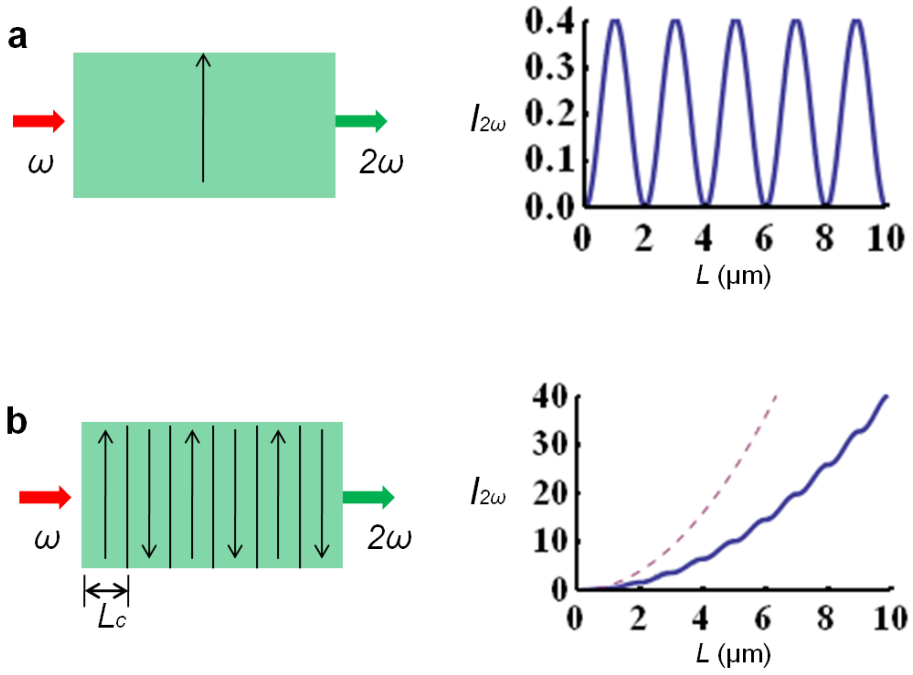

Figure 1.4: Spatial evolution of the second harmonic intensity from (a) a non-phase-matched crystal and (b) a quasi-phase-matched crystal. The dashed line in (b) represents the perfect phase-matching situation.

In order to obtain constructive interference over longer distances, some kind of phase-matching is required to maintain a fixed phase relation between the generated waves and the nonlinear polarization. This allows for the incident energy to be continuously transferred from the fundamental to the SH waves. With the quasi-phase-matching method, the nonlinear crystal axis is flipped at regular intervals, for example, by periodically poling a ferroelectric crystal. This allows the polarization response of the crystal to be shifted back in phase with the pump by reversing the nonlinear susceptibility. In this way, one can get a SHG signal that grows quadratically with the number of nonlinear domains (See Figure 1.4 b).

1.3 Phase-matching in random media

There are, essentially, two ways to meet the phase-matching conditions in different nonlinear structures to obtain efficient SHG. One way is by using the birefringence of the material [37]. The alternative is quasi-phase-matching by periodic pattern of the nonlinear susceptibility, as it was explained in the previous section [39-41]. However, these techniques are limited by the modest range of linear and nonlinear properties of natural materials, or require the complication of producing artificial structures or materials. Some ferroelectric crystals present naturally disordered structures that can provide relatively efficient light generation in an ultra-broad frequency range. The efficiency is lower

than that in perfectly phase-matched structures but can be much higher than that in non-phase-matched materials.

According to the phase-matching condition which is required for momentum conservation during the SHG process, the grating vectors for the domain distribution of the nonlinear material $\boldsymbol{k_g}$ should satisfy the vector equation $\boldsymbol{k_2}=\boldsymbol{2k_1}+\boldsymbol{k_g}$, where $\boldsymbol{k_2}$ is the wave vector of the SHG light, and $\boldsymbol{k_1}$ is the wave vector of the fundamental beam [42].

$$|\boldsymbol{k_2}| = \frac{4\pi}{\lambda_1} n(2\omega_1),\ |\boldsymbol{k_1}| = \frac{2\pi}{\lambda_1} n(\omega_1),\ |\boldsymbol{k_g}| = \frac{2\pi}{2D} \tag{1.3}$$

Here 2*D* is the domain periodicity, λ_1 and ω_1 are the wavelength and frequency of the fundamental beam, and $n(\omega_1)$ and $n(2\omega_1)$ are the refractive indices of fundamental and SH light.

In the case of nonlinear light generation from random materials, the wavelengths of the fundamental beam and SHG signal are fixed, which means fixed absolute values of $\boldsymbol{k_1}$ and $\boldsymbol{k_2}$. A scheme of the quasi phase-matching condition is shown in Figure 1.5. We may see that, the larger the angle between the fundamental beam and the SH one, the larger $\boldsymbol{k_g}$ is needed for phase-matching while $\boldsymbol{k_g}$ should take values between [43]:

$$|\boldsymbol{k_2}| - 2|\boldsymbol{k_1}| \leq |\boldsymbol{k_g}| \leq |\boldsymbol{k_2}| + 2|\boldsymbol{k_1}| \tag{1.4}$$

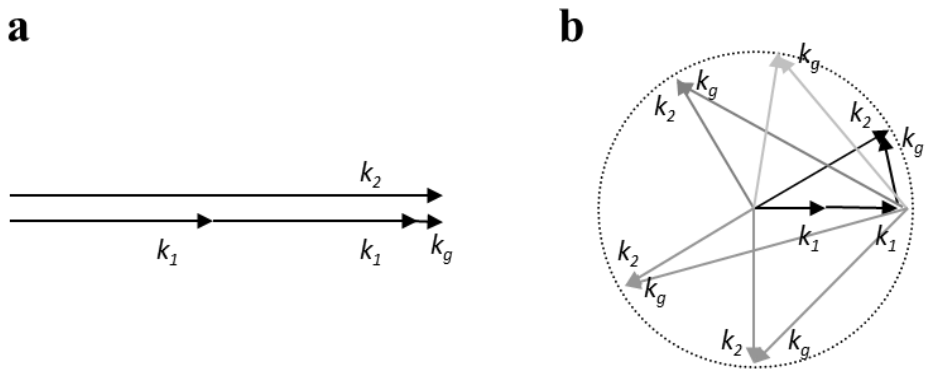

Figure 1.5: Schematic of the phase-matching relation between $\boldsymbol{k_1}$, $\boldsymbol{k_2}$, and $\boldsymbol{k_g}$ in the case of SHG in disordered media. (a) Collinear SHG. (b) Non-collinear SHG.

The SHG from disordered media grows linearly with the material length along the fundamental beam path (See Figure 1.6) [44].

To obtain a higher SH intensity from a random structure, besides increasing the material length, a better understanding of the relation between the SHG and the structure of the nonlinear random media is needed, so that the SHG efficiency can be optimized by modifying the random structure [45]. Moreover, with the wave-front shaping method, it is possible to concentrate the SHG after the disordered nonlinear structure, providing a new way to improve the SHG efficiency without modifying the random structure [46].

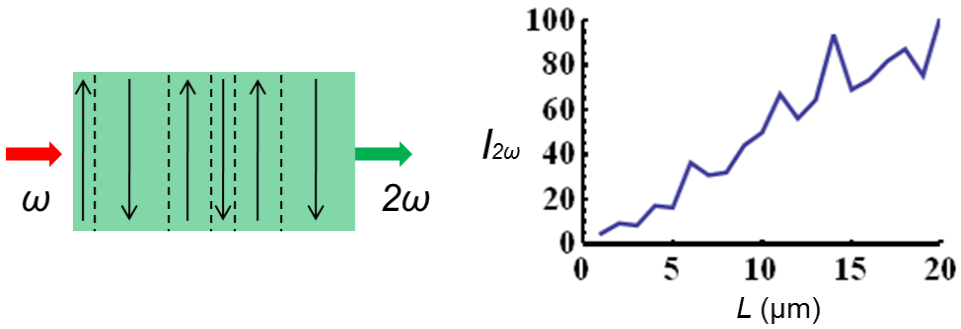

Figure 1.6: Spatial evolution of the second harmonic intensity from a disordered crystal.

1.4 Thesis summary

As indicated, light generation and propagation in random media is unavoidable in nature and frequently encountered. The coherence in the propagation and generation of light in such random media has been thoroughly studied leading to new applications such as coherent backscattering microscopy, random lasing and opaque lenses. When we consider the non-linear interaction in such random media, the coherent character or not of the phase-matching between interacting waves may play a determining role in the characteristics of the generated light. The aim of this thesis is to elucidate the intricate nature of such interaction and to propose new paths to counteract the effect of randomness in disordered non-linear media.

The remaining chapters explore the nonlinear coherent effect in a random media with homogeneous refractive index but a random

distribution of nonlinear susceptibilities. Chapter 2 describes a theoretical model of the SHG from the whole random structure based on the interference of the single scattering from each domain of the structure, and this model successfully illustrates the relationship between the nonlinear light generation and the random structure. Chapter 3 reports a unique nonlinear light speckle pattern generated from a transparent nonlinear random structure. Chapter 4 first presents the experimental result of focusing the second harmonic speckle reported in chapter 3 by the wave-front shaping method, and then, with the theoretical model derived in chapter 2, demonstrates the different control behavior of the second harmonic light at different output angles.

Chapter 2

SHG from structures with random distribution of nonlinear domains

Many efforts have already been made to understand SHG phenomena in random structures, both, theoretically [44, 47-51], and experimentally [52-55]. One of the preferred materials for such studies is SBN. The SBN crystal is a material with high optical nonlinearity, in which randomly distributed anti-parallel ferroelectric domains are easily generated [56-60]. Despite the anti-parallel domain structure the refractive index is maintained constant across the crystal, resulting in a transparent material that has nevertheless a random distribution in the nonlinear susceptibility. The randomness in the nonlinearity in SBN can be used in nonlinear optical processes for generating waves in a long frequency-range with relatively high efficiency.

This chapter contains two main sections. In the first section we simulate the SHG from different random two-dimensional domain structures and find how the domain size and macroscopic degree of polarization of the crystal affects the SHG. In the second section we report on the experimental SHG from the random SBN crystal. Then, comparing the SHG patterns from several SBN crystals after different electric field poling or thermal annealing treatments, the domain structure, for instance, the polarization distribution situation, is predicted by comparing the experimental and simulation results. Some studies on difference frequency generation (DFG) are also reported.

2.1 Theory

In order to understand the relation between the random domain structure and the second order light generation, we have implemented a theoretical study and simulation of the SHG from different structures. We consider a crystal structure characterized by a homogeneous refractive index but featuring random changes in the second order nonlinear susceptibility. More specifically, we focus our discussion in a structure similar to the one that can be found in ferroelectric crystals such as SBN. In such crystals, long domains are formed along the crystallographic c-axis with antiparallel orientation. In the case of SBN, the size and position of the domains are usually randomly distributed (See Figure 2.1). A random distribution can also be introduced in other

types of crystals, such as for instance, $LiNbO_3$ by electric field poling with designed patterns.

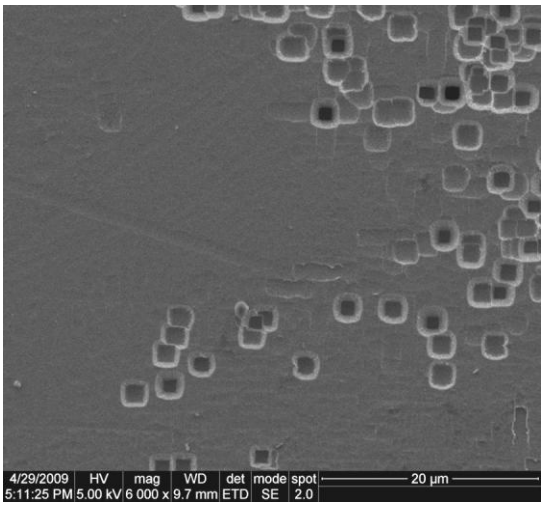

Figure 2.1: A SEM image showing the domains in the c-plane of a room temperature poled SBN crystal whose surface is chemically etched.

The elongated shape of the domains implies that the nonlinear light emission from a fundamental beam propagating perpendicular to the c-axis is mostly confined to the plane perpendicular to the c-axis, which is called the c-plane [48, 61].

2.1.1 SHG from one single domain

We first assume a rectangular domain of dimensions L_x, L_y, and L_z, embedded in a linear medium with the same refractive index. In order

to simplify the theoretical discussion, we restrict our analysis to the two-dimensional (2D) plane perpendicular to the c-axis (c-plane), by considering a fundamental beam propagating in such plane with its polarization parallel to the c-axis, and the polarization of the second harmonic light is also along the c-axis. We describe the c-plane with *x*-*y* Cartesian coordinates. Within the Green function formalism, we obtain an analytical expression for the SHG electric field amplitude $E^{2\omega}$ from one single domain with dimensions L_x and L_y along the *x* and *y* directions, respectively, and located at position (*x*,*y*) can be expressed as [45]:

$$E_{(x,y)}^{2\omega} = \frac{2\omega^2 e^{\frac{i2\omega n_{2\omega} r}{c}}}{c^2 \pi r} d_{eff} E^{\omega} E^{\omega} e^{i(x\Delta k_x + y\Delta k_y)} L_x L_y \quad (2.1)$$
$$sinc(\Delta k_x L_x/2) sinc(\Delta k_y L_y/2)$$

where ω is the fundamental frequency, E^{ω} is the fundamental electric field amplitude, d_{eff} is the effective component of the second order nonlinear susceptibility $\chi^{(2)}$ and *r* the distance to the observation point. The phase mismatch between the fundamental and SHG light in the *x* direction is $\Delta k_x = 4\pi(n_{2\omega}\cos\phi_{2\omega} - n_{\omega}\cos\phi_{in})/\lambda_{\omega}$ and the phase mismatch in *y* direction is $\Delta k_y = 4\pi(n_{2\omega}\sin\phi_{2\omega} - n_{\omega}\sin\phi_{in})/\lambda_{\omega}$, n_{ω} and $n_{2\omega}$ are the refractive indices of fundamental and SH light, λ_{ω} is the fundamental wavelength, and $\phi_{2\omega}$ and ϕ_{in} are the SHG output angle

and fundamental incident angle, respectively, as shown in Figure 2.2. Without loss of generality, we take $\phi_{in} = 0$.

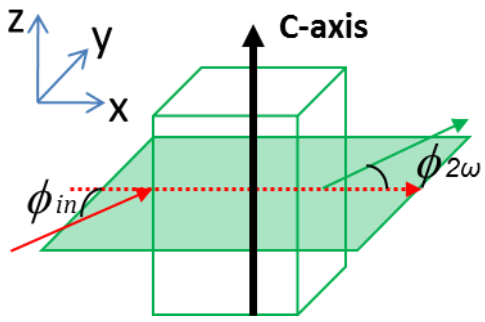

Figure 2.2: Scheme of a three dimensional single domain.

From Eq. 2.1, the second harmonic intensity (SHI) under plane wave input is

$$I_{2\omega} = dL_x^2 L_y^2 \, sinc^2\left(\frac{\Delta k_x L_x}{2}\right) sinc^2\left(\frac{\Delta k_y L_y}{2}\right) \tag{2.2}$$

We denote $d = 8\omega^4 n_{2\omega} d_{eff}^2 I_\omega I_\omega / c^5 \pi^2 r^2 n_\omega^2 \varepsilon_0$, and I_ω is the fundamental beam intensity. We assume the fundamental beam at wavelength 1064 nm, and therefore the SHG at 532 nm. We take the extraordinary refractive index of the material as that of the SBN crystal $n_{1064\text{nm}} = 2.22$ and $n_{532\text{nm}} = 2.32$ [45], which gives a coherence length for the SHG propagation in the same direction as the fundamental of $L_c = \pi / \Delta k =$

2.68 μm. In such case, $\Delta k_x = 0$ for $\phi_{2\omega} = 16.8°$. The SHI in such direction can be simplified into

$$I_{2\omega} = \frac{4dL_x^2}{\Delta k_y{}^2} sin^2\left(\frac{\Delta k_y L_y}{2}\right) \tag{2.3}$$

Thus, the SHI will follow a quadratic growth with the crystal length L_x, and it will oscillate periodically with L_y (See Figure 2.3). This condition is also called Cerenkov phase-matching [62-65]. In the same way, in the case of collinear SHG ($\phi_{2\omega} = 0°$), $\Delta k_y = 0$. The intensity will have an expression as in Eq. 2.3 but with a permutation of the subscripts *x* and *y*. The SHI will follow a quadratic growth with the crystal width L_y, and it will oscillate periodically with the crystal length L_x (See Figure 2.3). This oscillation of the intensity with the crystal length corresponds to the so called Maker fringe effect [66,67].

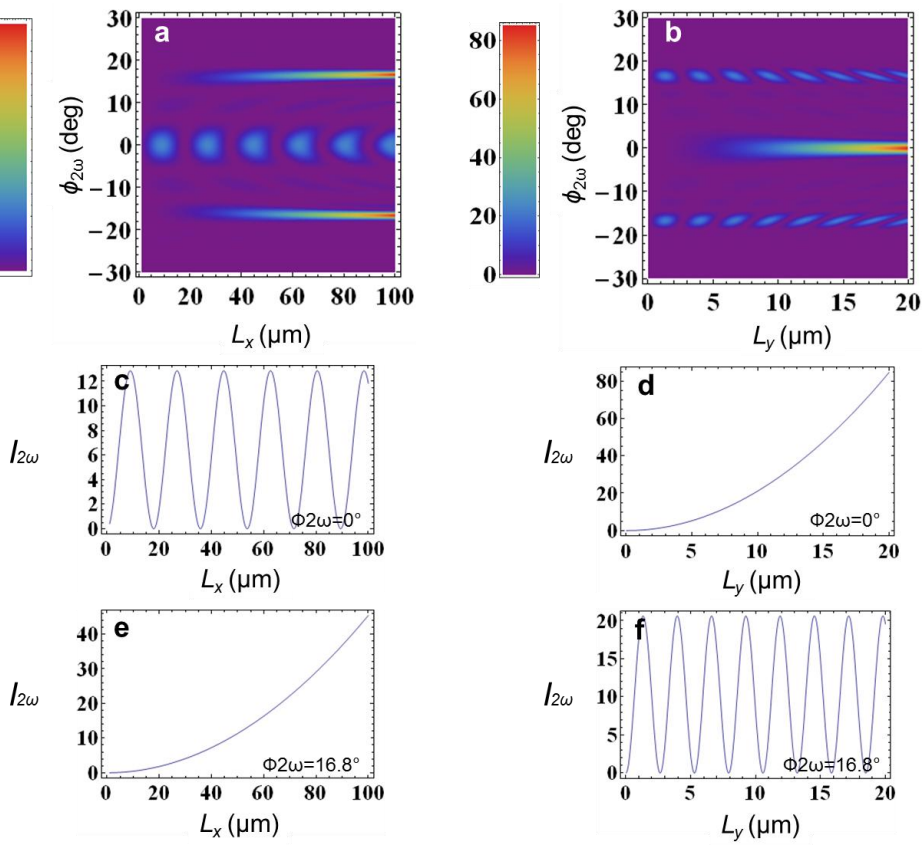

Figure 2.3: Spatial distribution of the SHI from a homogeneous crystal of 2.1 μm width, and variable crystal length (a), and the SHI change with the crystal length at output angle 0° (c) and angle 16.8° (e). Spatial distribution of the SHI from a homogeneous crystal of 18 μm length, and variable crystal width (b), and the SHI change with the crystal width at output angle 0° (d) and angle 16.8° (f).

These effects are due to the boundaries of the nonlinear material. They can be applied both to the microscopic domains inside the crystal or to a macroscopic homogeneous crystal if we neglect the effect of the refractive index change with respect to the surrounding medium. In the last case, we will see later that the effect persists even after we

introduce randomness to the inner structure. On the other hand, for SHI at any angle $\phi_{2\omega}$, for which neither Δk_x nor Δk_y is 0,

$$I_{2\omega} = \frac{16d}{\Delta k_x{}^2 \Delta k_y{}^2} sin^2\left(\frac{\Delta k_x L_x}{2}\right) sin^2\left(\frac{\Delta k_y L_y}{2}\right) \tag{2.4}$$

which can be rather weak compared with the quadratic growth in the collinear and Cerenkov cases. In general, when we introduce randomness in the structure, the boundary effect in the macroscopic crystal will be negligible in these directions.

We now compare the SHG profiles from square domains with different side lengths. From Figure 2.4 and Figure 2.5, we can see that bigger domains generate narrower peaks with higher intensity in the collinear and Cerenkov directions, while the SHG from smaller domains is weaker and more wide-spread in all directions.

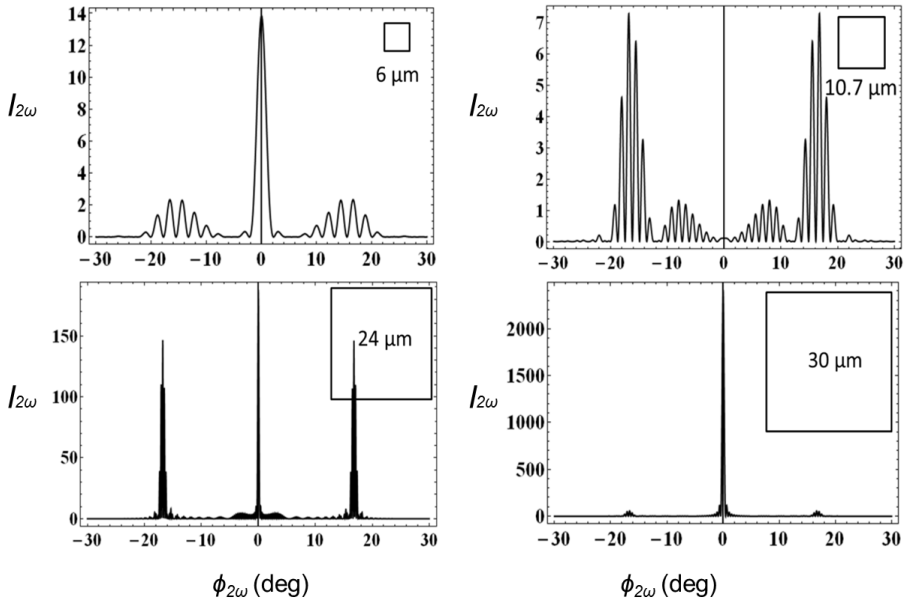

Figure 2.4: SHG from a single domain with different domain side lengths.

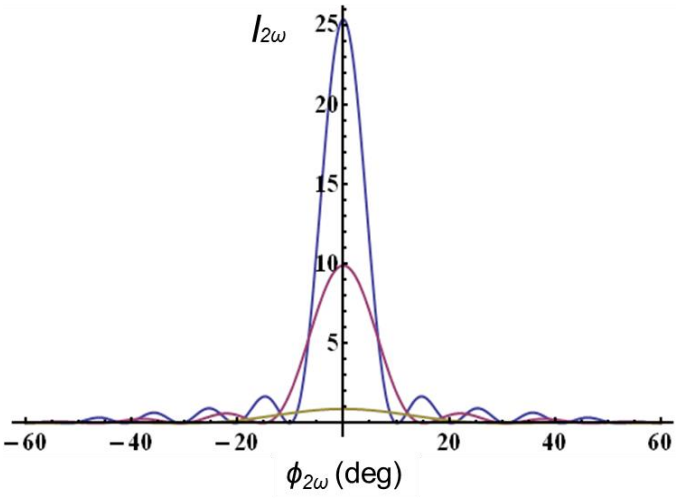

Figure 2.5: SHG from single square domains with different side lengths L. Blue: L=3 μm. Red: L=2 μm. Yellow: L=1 μm.

The SHG spatial distribution at the far field from a random structure can be calculated from the sum of the SHG from different domains. In this way, we can predict that a random structure with bigger domains will generate SHG more concentrated around the forward direction, and a random structure with smaller domains will generate SHG more wide-spread in all directions.

Besides, it is useful to notice that the whole crystal can be seen as a big uniform domain. We call this contribution to SHG the boundary effect. From the discussion above, we know that the boundary effect only generates SH light in the collinear or Cerenkov angle, while it has little impact on the SHG in other directions. Moreover, both the collinear and the Cerenkov SHG intensities oscillate periodically with the distance between the crystal boundaries perpendicular to the beam propagation or parallel to it, respectively. Notice also that the Cerenkov peak only appears in the case in which the fundamental light beam is illuminating the lateral faces parallel to the propagation direction. This is not the case in most experiments since the beam diameter is usually smaller than the crystal.

2.1.2 SHG from a random distribution of domains

Once the SH electric field from a single domain has been calculated, the SH electric field from the whole structure can be obtained as the result of the interference of the SHG from each domain. Thus, if we

assume that there are N domains distributed in the random structure, the position of the n^{th} ($1 \leqslant n \leqslant N$) domain is (x_n, y_n), and $E_{x_n,y_n}^{2\omega}$ is the SH electric field from the n^{th} domain, we can write the SH electric field from the whole structure:

$$E^{2\omega} = \sum_{n=1}^{N} E_{x_n,y_n}^{2\omega} \tag{2.5}$$

In the crystal structure considered, the absolute value of the effective nonlinear susceptibility is constant and only its sign changes for domains with opposite polarization. If we take P_n with value 1 or -1 as the sign given by the polarization of domain n, and the domain size is L_{x_n} and L_{y_n} along the x and y directions, from Eqs. (2.1) and (2.5), the SHG intensity (SHI) can be expressed as:

$$I_{2\omega} = d \left| \sum_{n=1}^{N} P_n L_{x_n} L_{y_n} e^{i(x_n \Delta k_x + y_n \Delta k_y)} sinc\left(\frac{\Delta k_x L_{x_n}}{2}\right) sinc\left(\frac{\Delta k_y L_{y_n}}{2}\right) \right|^2 \tag{2.6}$$

As opposed to the single domain (homogeneous crystal) case, for the random regime, even when the domain size is uniform and L_{x_n} and L_{y_n} are fixed, the randomness in the polarization leads to an $I_{2\omega}$ that

becomes proportional to the domain number N (Eq. 2.6). As shown in Figure 2.6, on average the SHI at any angle grows linearly with the beam path length in a random structure with random domain size and polarization.

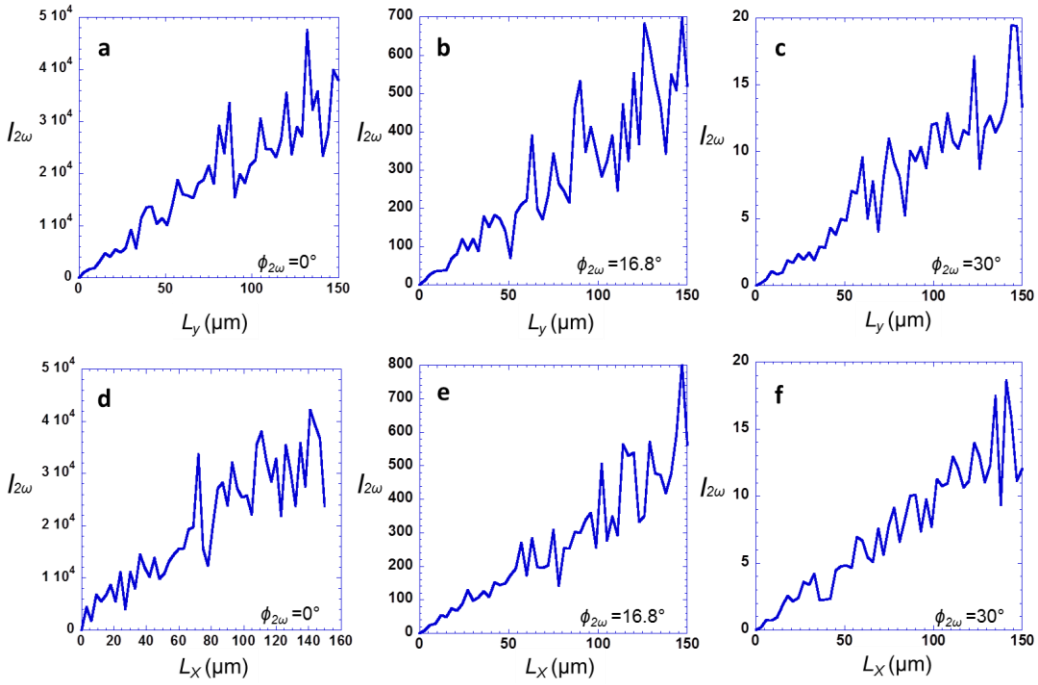

Figure 2.6: SHI growth with the random structure width at (a) 0° (b) 16.8° (c) 30°, and with length at (d) 0° (e) 16.8° (f) 30°, from a group of random domains scattered in a rectangular area whose length or width is fixed at 150 μm. The domain sizes are random between 1 and 3 μm. Each plot corresponds to the average over 20 different realizations of the randomness.

2.1.3 SHG from a random crystal structure

When the random domain distribution is combined with a well-defined boundary between the nonlinear material and the surrounding linear medium (air), as for random crystal structure in SBN, the contribution to the SHI is from, both, the random structure and the crystal boundary. As a result, the intensity will show at the same time features from a homogeneous nonlinear structure with the dimensions of the whole crystal (See Figure 2.3) and from a random structure given by the disordered domain substructure (See Figure 2.6).

From Figure 2.7a and Figure 2.7d, SHI in the forward direction (0°) grows between linear (Figure 2.6a) and quadratic (Figure 2.3d) with the structure width, and the effect of the structure length is also a linear growth (Figure 2.6d) but superposed with a periodical oscillation as seen in Figure 2.3c. On the other hand, as shown in Figure 2.7b and Figure 2.7e, the SHI in the Cerenkov direction (16.8°) grows between linear (Figure 2.6e) and quadratic (Figure 2.3e) with the structure length, and it oscillates periodically with the structure width (See Figure 2.3f) while at the same time it exhibits an average linear growth (See Figure 2.6b). The combination of the contribution from the boundaries and the one from the random structure exhibits a slight deviation from the linear growth. For SHI at any other output angle, for which neither Δk_x nor Δk_y is 0, we see that the SHI is rather weak compared with the SHI in the collinear and Cerenkov angles. In all such cases the SHI grows linearly with, both, the structure width and

length, as seen in Figure 2.7c and Figure 2.7f. This indicates that when one introduces randomness in the structure, the boundary contribution is negligible in all such directions.

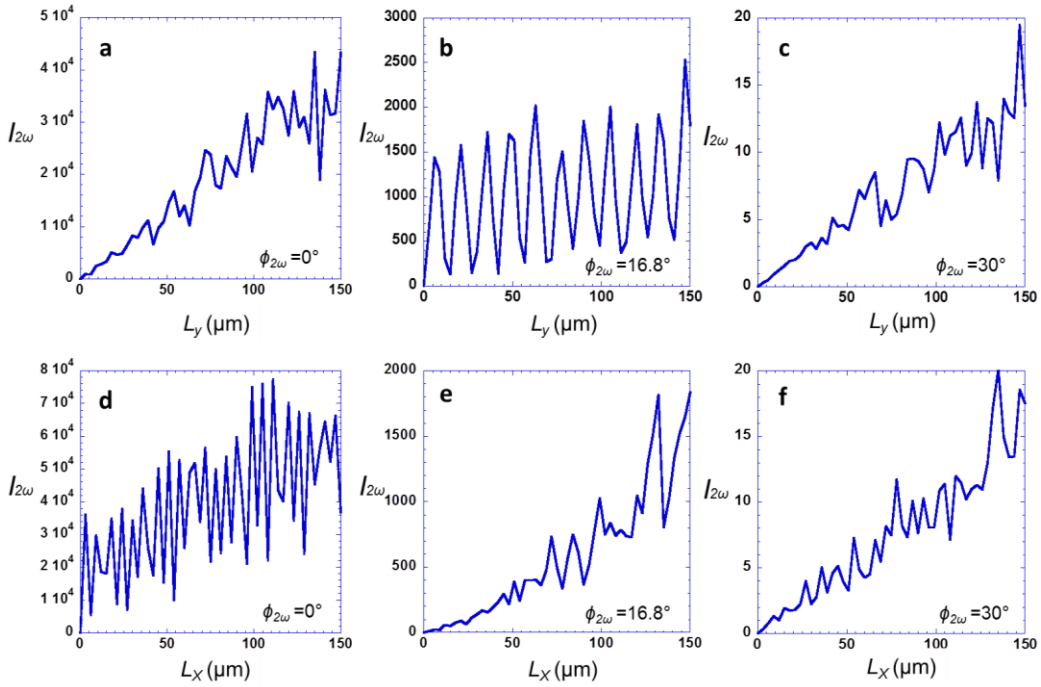

Figure 2.7: SHI growth with the rectangular random crystal width at (a) 0° (b) 16.8° (c) 30°, and with length at (d) 0° (e) 16.8° (f) 30°, when the random crystal has a fixed length of 150 μm or a fixed width of 150 μm, respectively. The domains are with random sizes between 1 and 3 μm. The random domains with opposite polarizations are approximately in a 1:1 ratio. Each plot corresponds to the average over 20 different realizations of the randomness.

In what follows, we consider the SHG profile from several random structures. Firstly, if we introduce opposite polarization domains in a homogeneous structure, we find that we are able to achieve a much stronger collinear SH peak than that from the boundary effect from a

one polarization large single domain. This SH peak is due to the constructive interference of the SHG from each random domain [48], so we call it the random effect.

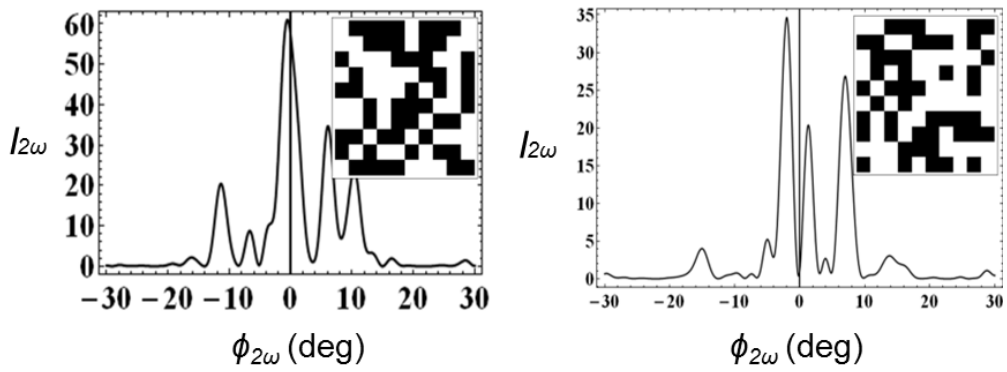

Figure 2.8: Simulation of SHG from random structures composed of 10*10 random domains each with the same size 0.6 μm*0.6 μm. Due to the different polarization distribution, different SHI profiles are generated. The random domains with opposite polarizations are approximately half by half.

While keeping the whole structure´s size, if we introduce more and smaller random domains in the structure, when the domain size is small compared to the coherence length, in the forward direction the SHG from each domain spreads from the forward direction and scatters around, so the SHG profile from the whole structure follows the same tendency (See Figure 2.8). Depending on the interference of the SHG from each domain, the SHG peak in the collinear direction can be either enhanced or suppressed compared to the SHG peak from the homogeneous structure. We may conclude that in the random structure,

the random effect in the crystal can overtake or wash out the boundary effect.

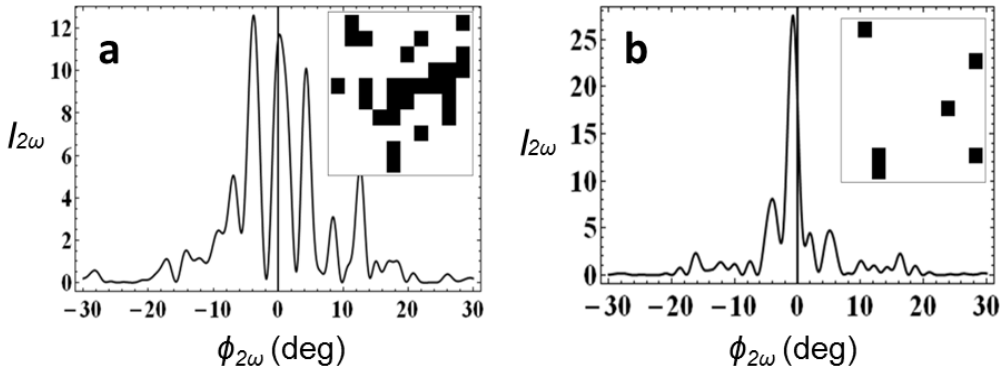

Figure 2.9: Simulation of SHG from random structures composed of 10*10 random domains each with the same size 0.6 µm*0.6 µm. The random domains with positive polarization take approximately (a) 20% and (b) 10% of the whole structure area.

If we decrease the level of randomness of the structure as shown in Figure 2.9, where the random domains with positive polarization separately take up approximately 20% and 10% of the whole structure area, we find the SHG in the higher level disordered structure spreads wider (See Figure 2.9a) than in the case where the level of randomness is smaller (See Figure 2.9b). In that case the SHG profile is very close to the one from a homogeneous structure exhibiting a SH peak collinear with the fundamental beam and negligible SHG in other directions.

We have also considered configurations where we further reduce the domain sizes while keeping the whole structure´s size, until there are

many very small anti-parallel random domains distributed in the structure, whose sizes are ten orders of magnitude smaller than the coherence length in the forward direction. However, although the SHG from this structure with the largest number and smallest domains has decreased significantly, the SH peak in the collinear direction can still be seen under a certain proportion of the random domains with opposite polarizations (See Figure 2.10).

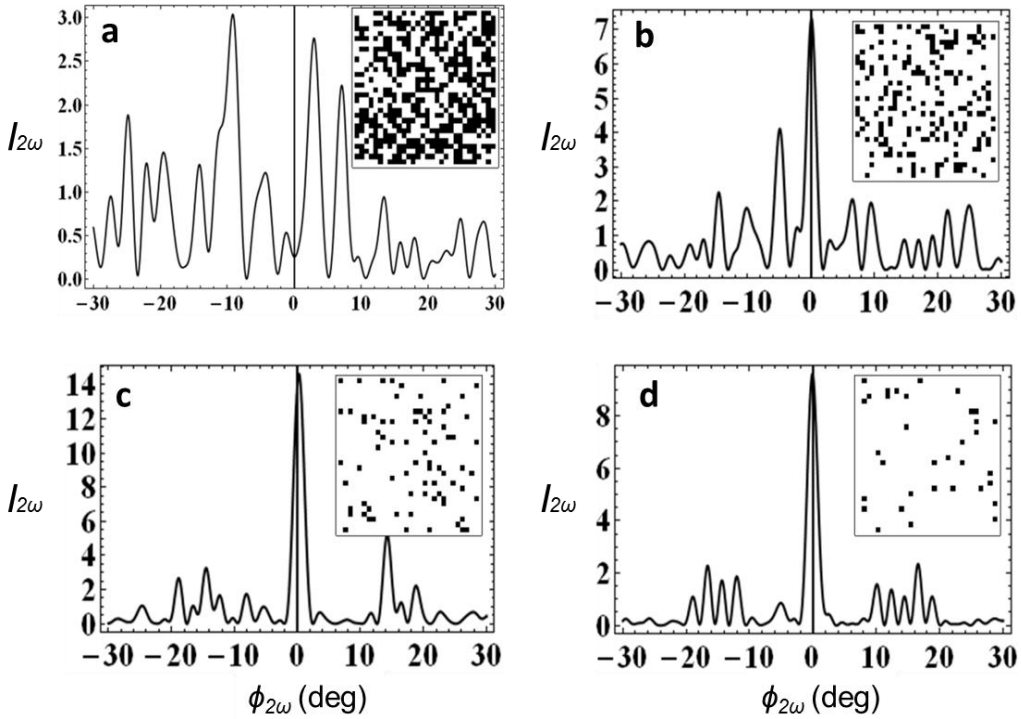

Figure 2.10: Simulation of SHG from random structures composed of 30*30 random domains all of them with the same size 0.2 μm*0.2 μm. The random domains with positive polarization take approximately (a) 50% (b) 20% (c) 10% and (d) 5% of the whole structure area.

When the domain sizes are reduced to a hundred orders of magnitude smaller than the coherence length in the forward direction, and the random domains with opposite polarizations are approximately half by half, the SHG becomes very weak and almost negligible (See Figure 2.11a). In this case, the structure with very small domains distributed randomly in opposite polarizations can be taken as centro-symmetric. However, if we increase the number of domains pointing in one direction to the domains pointing in the opposite direction, the structure can not be taken as centro-symmetric any longer, and it may exhibit the SHG as from a homogeneous structure (See Figure 2.11b).

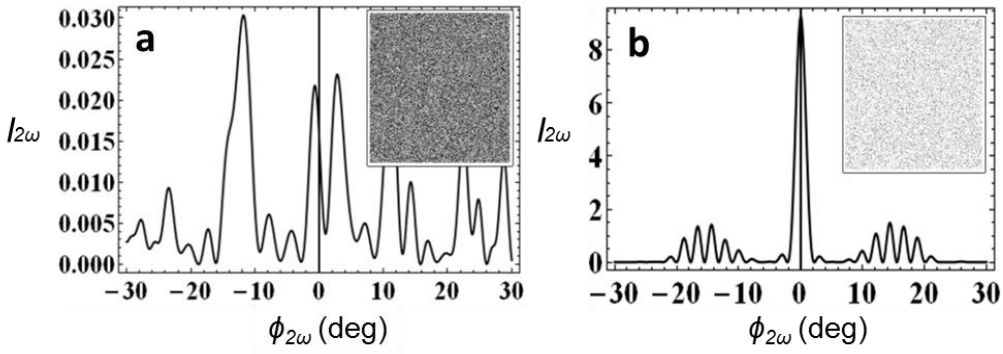

Figure 2.11: Simulation of SHG from random structures composed of 400*400 random domains all of them with the same size 15 nm*15 nm. The random domains with positive polarization take approximately (a) 50% and (b) 10% of the whole structure area.

2.2 Experimental results

2.2.1 SBN crystal properties

The SBN crystal is a ferroelectric, transparent material (See Figure 2.12) that usually displays a high number of randomly distributed anti-parallel domains. The ferroelectric phase takes place at temperatures below its Curie point around 75 ℃ [68]. The ferroelectric to para-electric phase transition changes the symmetry from tetragonal 4/mmm into 4mm by shifting off all metal ions along the tetragonal polar axis [69, 70]. The SBN crystal has proved to exhibit a high optical nonlinearity and has been reported to have promising applications in photonics, data storage or switching [71, 72].

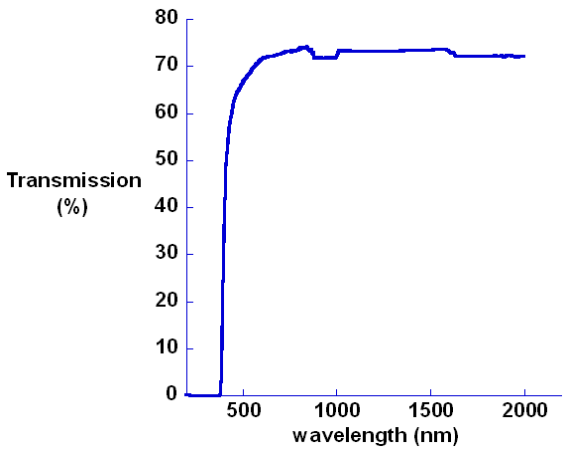

Figure 2.12: The transparency of an SBN crystal for different wavelengths.

Due to its ferroelectricity one is able to change the SBN random domain structure by poling and/or thermal treatments. In this thesis we have considered the following treatments:

1) Thermal treatment (Annealing): The SBN crystal is heated slowly (about 0.4 ℃/min) to a temperature between 160 ℃ and 260 ℃, and then cooled down slowly to the room temperature. It is found that regardless of its previous state, the SBN crystal after such a thermal treatment shows a structure with random domains of sizes much smaller compared to the coherence length of SH light in the forward direction [73], and the higher the temperature, the smaller would be the domains obtained.

2) Room temperature poling: At room temperature, an electric field over 200V/mm is applied along the c-axis of the crystal. It is found that such room temperature poling of the SBN crystal takes effect only after a thermal treatment and will mostly yield a quasi-mono domain crystal, whose polarization direction is along the electric field applied.

3) Thermal poling: The crystal is heated to a high temperature above the Curie point, an electric field over 200 V/mm is applied along the c-axis of the SBN crystal and the field is maintained while the crystal is cooled down to room temperature [74]. The thermal poling of SBN can result in a mono domain crystal whose polarization points along the electric field applied.

4) Reverse poling: An electric field is applied along the reverse direction of the previous poling. Such reverse poling of the SBN crystal

will lead to random domains with the reverse polarization, and under proper voltage, the average random domain size is close to the coherence length of SH light in the forward direction. After a reverse poling, a strong SHI can be achieved in most directions in the c-plane. Thus, the SHG is most efficient after the reverse poling treatment. The structure of SBN crystal after the reverse poling treatment is almost not modified by subsequent poling treatments, and it can only be changed by thermal treatments.

There are different ways to visualize the domain structure in ferroelectric crystals [75]. Surface modifications such as chemical etching are direct but destructive [76], since the positive and negative polarized domains have different etching behaviors, imaging of the resulting topography after etching will represent the ferroelectric domain structure. On the other hand, optical methods which are non-contact and non-invasive, are mostly limited by the diffraction limit and their resolution is, typically, not better than 1 μm [75]. For example, polarization microscopy with an electric field applied to the ferroelectric structure, which introduces refractive index difference between domains of different polarizations, causes retardation leading to a contrast in the observed image [77]. Another example is SHG microscopy taking advantage of the phase difference of the SH light from domains of different polarizations, and the domain structure information can be obtained by the interference of the SHG from the ferroelectric crystal and from a uniform SHG plate [78, 79].

In this thesis, we visualize the structure of SBN crystal using the chemical etching method after different treatments. Usually, the imaging of SBN domains requires two steps: firstly, a chemical etching of the SBN crystal in HF (48%) for about 15 minutes [80] must be carried out and then cleaned with large amounts of water and 2-propanol. Secondly, the chemically etched SBN crystal is observed under an optical microscope or scanning electron microscope (SEM). In this way, we are able to identify the shape of the domains (See Figure 2.13a).

Interestingly, the SHG produced by a wide beam can be used to visualize the domains in a similar way as in SHG microscopy [81]. In this case the fundamental beam is not raster scanned over the crystal, but illuminates the entire area being imaged. The image of the crystal surface is projected with a macro objective on a CCD sensor. The resultant image reveals the inner random domain morphology of the crystal. As an example, Figure 2.13b shows the needlelike domains randomly distributed along the c-axis.

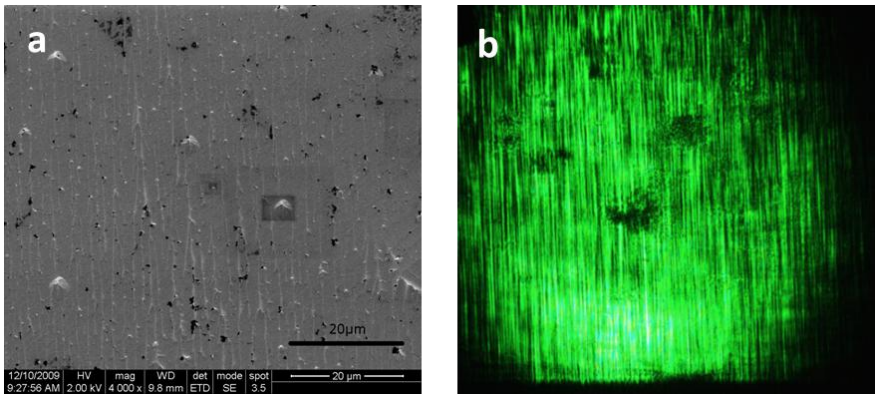

Figure 2.13: The viewing of the random domains of SBN crystal. (a) SEM image of chemically etched SBN crystal, note that, the cross-section of domains is square-shaped. (b) SHG image of SBN revealing the needlelike domains along the c-axis.

2.2.2 SHG from SBN crystal

We may distinguish, mainly, two profiles on the emission of SHG depending on the direction of propagation of the fundamental beam relative to the c-axis. If the fundamental beam propagates along the c-axis of the SBN crystal, the SHG emission is cone-shaped. When the fundamental beam propagates perpendicular to the c-axis, SHG is on the plane perpendicular to the c-axis [56]. Most of the SHG considered in this thesis corresponds to the latter case.

The disordered domains with different sizes and located at different positions in the SBN crystal provide a large number of grating vectors for random "phase-matching". Such crystal configuration can be used in nonlinear optical processes for generating waves at different frequencies with relatively high efficiency (See Figure 2.14).

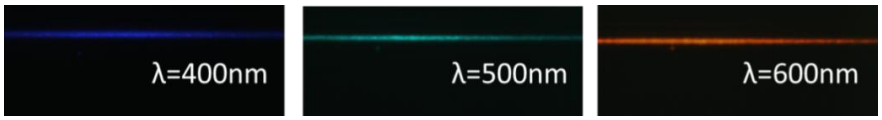

Figure 2.14: The SHG from SBN crystal with different wavelengths.

We built the experimental set up as shown in Figure 2.15, in order to investigate the SHG emission of the SBN crystal. We used a Q-switched Nd:YAG laser system at the wavelength of 1064 nm with a repetition rate of 10 Hz, and pulse duration close to 6 nanoseconds. Two lenses were used to generate a collimated fundamental beam directed perpendicular to the c-axis of the SBN crystal. The SHG from the crystal was focused by a lens placed right after the crystal, and measured at the focal plane of the lens to study the intensity distribution at the far field. The measurements were carried out using either a photodiode or a photomultiplier installed on a translation stage, or with a CCD sensor, depending on the strength of the SHG signal.

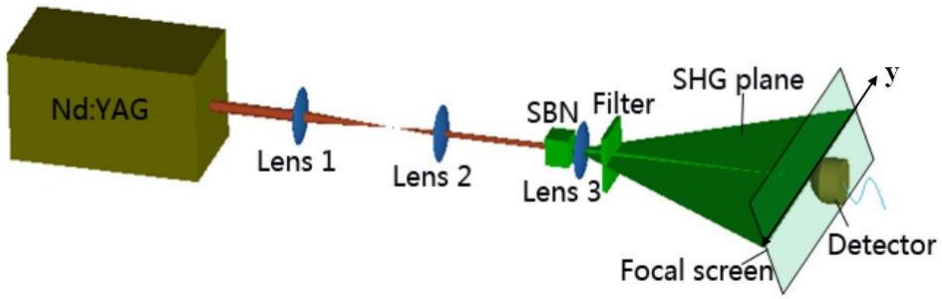

Figure 2.15: Scheme of the SHG detection of an SBN crystal.

2.2.3 Collinear peak in the SHG from SBN crystal

By measuring the SHG spatial distribution along the y direction as shown in Figure 2.15, we have found a SHG peak in the direction of the fundamental beam. Figure 2.16 shows the SHG peak taken by a CCD camera from a room temperature poled SBN crystal and another one annealed from 180 ℃ to room temperature, respectively. The same peak has been detected also in one SBN crystal after a reverse poling treatment (See Figure 2.17), and we find the SHG peak in the collinear direction oscillates with the incident beam path length in the crystal when we rotate the crystal along its c-axis.

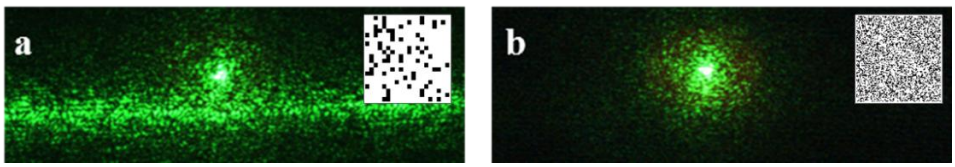

Figure 2.16: The SHG peak in the forward direction from (a) poled and (b) annealed SBN crystals. The square insets are schematic representations of the random square-domain structure in the c-plane of SBN crystal.

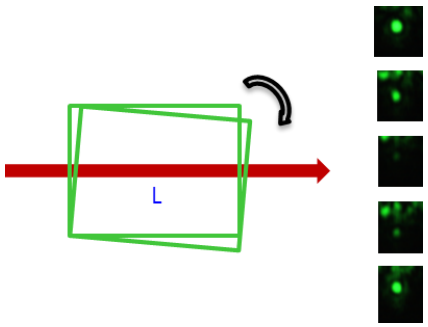

Figure 2.17: The Front peak intensity oscillates as the light path changes in the crystal when the crystal is rotated.

We find that the SHG peak intensity also oscillates with the temperature (Figure 2.18). We attribute this periodic oscillation to the coherence length change of the SH light as the refractive index of the crystal changes with the temperature. All this indicates that the peak has the same origin as the SHG that would be found in a homogeneous crystal.

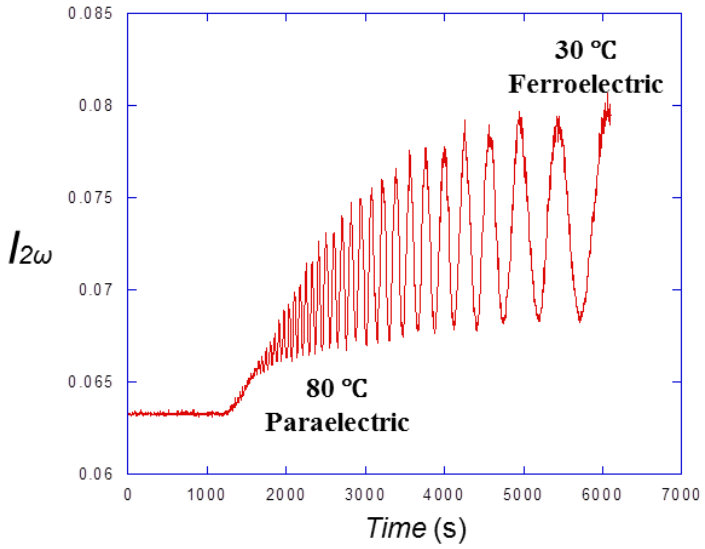

Figure 2.18: Oscillations in the SHG emitted in the direction of the fundamental beam as the crystal is cooled down from a temperature just above the Curie temperature. The oscillations are due to a Maker fringe effect with the change of refractive index dispersion with the temperature.

The SHG peak from the crystal boundary effect appears in the direction of the fundamental beam, and the SHG due to the random structure follows the random quasi phase-matching condition (See Chapter 1, section 1.3). When the fundamental beam is not on the c-plane, we may clearly distinguish the SHG peak by the crystal boundary effect from the random SHG as shown in Figure 2.19a. We can see an intense SHG line due to the random effect in the c-plane and a SH peak below the line due to the crystal boundary effect in the fundamental beam direction. In this case the SHG peak is weaker than the SHG distributed in the c-plane. In the case in which the fundamental beam is on the c-plane, the weaker SHG peak will be buried into the SHG line, and we will not be able to distinguish it (Figure 2.19b).

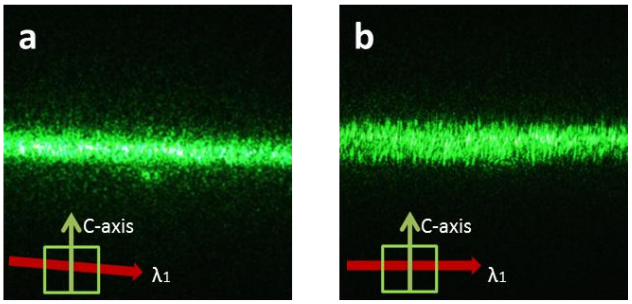

Figure 2.19: The SHG from a reversely poled SBN crystal. (a) Fundamental beam not in the c-plane. (b) Fundamental beam in the c-plane.

Experimentally, we have also verified that the SHG intensity has a linear growth with the beam path length in the SBN crystal. We use a trapezium shaped SBN crystal whose parallel sides are along the beam propagation direction. As we move the crystal on a translation stage in the transverse direction, the beam path length in the crystal changes. We measure the SHI from SBN crystal at an arbitrary angle (Figure 2.20).

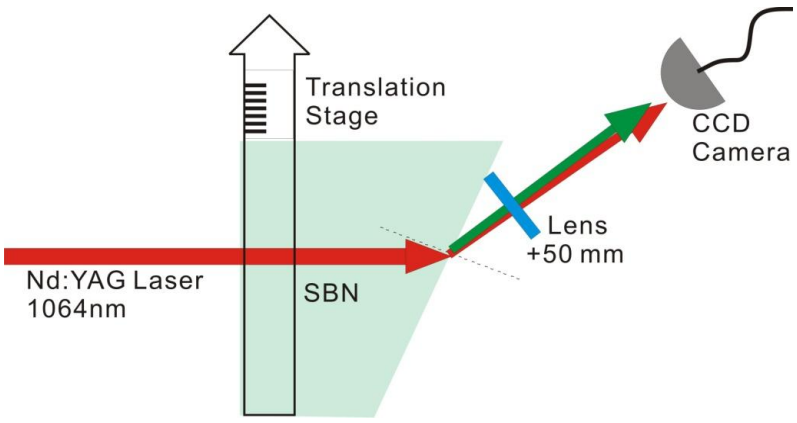

Figure 2.20: Scheme of experimental set up of the SHI linear growth with the beam path length in the SBN crystal.

It is found that the SHI in the area not including the SH peak grows linearly with the beam path length (See Figure 2.21), which shows that the measured SHG is only contributed by the random structure effect. On the other hand, the SHI at the area which includes the SH peak would grow linearly with the beam path length while showing an oscillating behavior on top of the linear growth, coming from the interference of the SH light contributions from both the random and the boundary effect. However, since the oscillation period is the coherence length of the SH light which is several microns, it is not possible to achieve this precision with the experimental setup shown in Figure 2.20. In order to see this oscillation, we can rotate the crystal (See Figure 2.17) or change the crystal refractive index (See Figure 2.18).

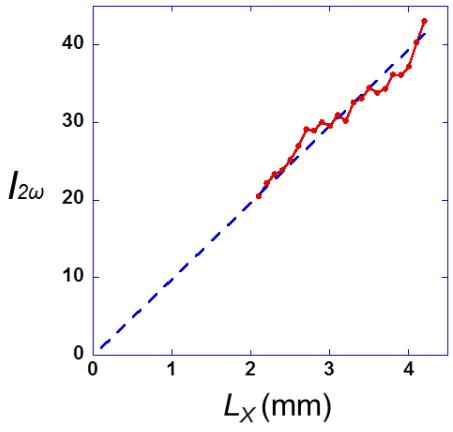

Figure 2.21: Scheme of the SHI growth with the beam path length in the SBN crystal. The measured SHI area doesn´t include the SH peak.

2.2.4 Comparison of the SHG profile from SBN crystal after poling and thermal treatments

The SBN crystal after different treatments exhibits different SHG spatial distributions on the c-plane. We compared the SHG of poled, reversely poled and thermal treated SBN crystals. The intensity and profile of the SHG are measured with the experimental set up shown in Figure 2.15.

For an SBN crystal after the thermal poling treatment, the SHG shows a clear peak in the forward direction with negligible signal in any other direction (See Figure 2.22), which fits well with the SHG from a homogeneous structure illustrated in Figure 2.5. This implies that after the thermal poling treatment, the crystal is a homogeneous structure which can be regarded as a big single domain whose polarization points along the direction of the electric field applied.

If we make an annealing treatment to the SBN crystal, we find that SHG is negligible in all directions. This fits the SHG from a structure with very small random domains whose opposite polarizations yield an almost centro-symmetric structure as illustrated in Figure 2.11a. This indicates that, after the annealing, the SBN crystal has random domains much smaller than the coherence length of the SH light, and that the number of domains in each polarization direction is equivalent.

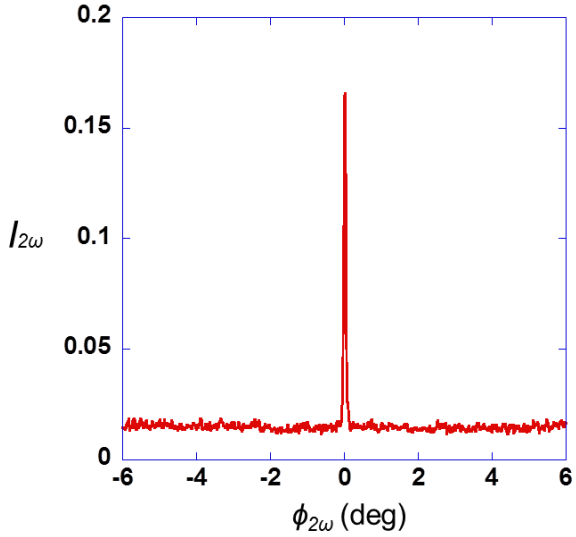

Figure 2.22: SHG distribution in the c-plane from an SBN crystal after the thermal poling treatment.

If we apply a room temperature poling to the annealed SBN crystal, we can observe strong SHG emission within a 10 degrees angular aperture in the forward direction (See Figure 2.23), as it has also been observed by other researchers [82]. This necessarily means that after a room temperature poling, though most of the domains are in the direction of the electric field applied, there are still a number of random domains with reverse polarization and dimensions on the order of the coherence length in the forward direction.

Starting with the previously poled structure, if we make a reverse poling by applying a reverse electric field, we see stronger SHG distributed within almost the same range as that of the poled crystal (Figure 2.23). Since the SHG distribution range largely depends on the domain size, we conclude that the domains created during the room

temperature poling and those created during the reverse poling have similar average sizes. However, the number of domains of dimension on the order of the coherence length is larger after the reverse poling. At the same time, the proportion of domains with opposite polarizations will be different. Besides, we are not able to improve the SHG from a reversely poled crystal by any thermal or poling treatment. The reversely poled crystal generates the highest SHG efficiency that we have achieved.

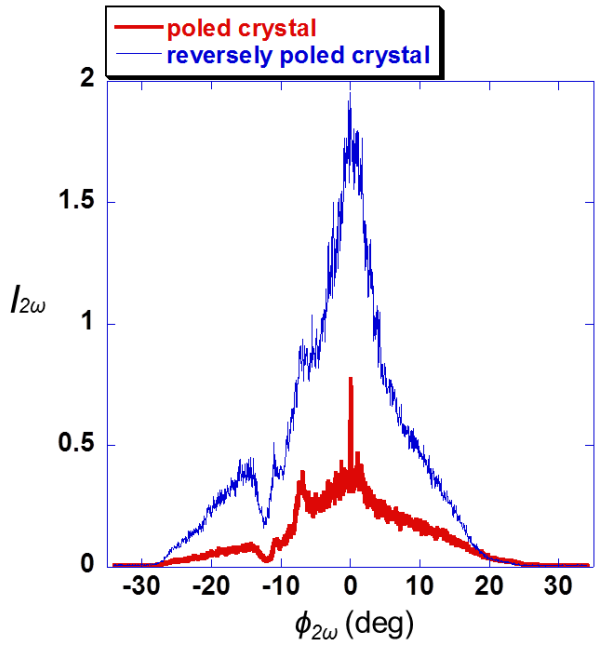

Figure 2.23: SHG of the SBN crystal after a room temperature poling and a reverse poling treatment.

Figure 2.24 shows how the SHG intensity in the forward direction changes during a poling process, with two electric field of opposite directions applied to SBN crystal in sequence. The maximum efficiency for the laser parameters used in this experiment, calculated by dividing the SHG power by the laser power, is around 0.0025%.

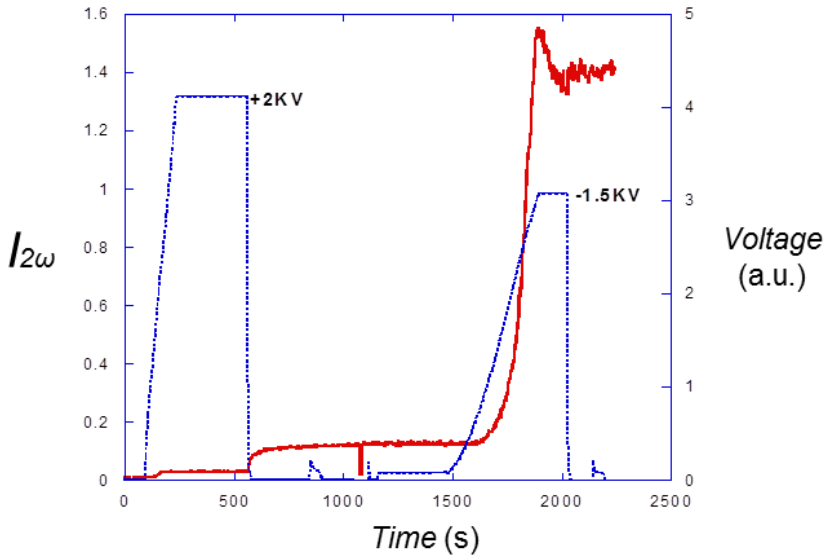

Figure 2.24: The SHG intensity increases when a reverse poling is applied to SBN crystal. Red solid line: SHG intensity. Blue dashed line: Voltage applied on SBN.

2.2.5 Difference frequency generation from SBN crystal

The simultaneous generation of sum, difference, and harmonics of two laser frequencies from a nonlinear SBN crystal has been reported by Horowitz, et al. [83]. Here, instead of focusing on the conversion

efficiency of the processes, we report a DFG with similar spatial distribution as the SHG from SBN crystals. We use part of the light from a frequency doubled Q-switched Nd-YAG laser as the pump (ω_p) at 532 nm. The other part of the light is frequency tripled and fed into an OPO to generate the idler beam (ω_i) for our experiment, which is tuned between 1120 nm and 1300 nm. In this way, the DFG signal (ω_s) produced by the SBN crystal has the wavelength between 900 nm and 1010 nm due to the energy conservation law, $\omega_p = \omega_i + \omega_s$. Both the Nd-YAG laser and the OPO are part of a commercial system (Coherent Vibrant). The pulses have a repetition rate of 10 Hz, pulse duration about 6 nanoseconds, and the beam diameter is 3 mm. The DFG from the crystal is focused by a lens placed right after the crystal, and measured at the focal plane of the lens to study the intensity distribution at the far field (Figure 2.25). The measurements are carried out using either a photodiode or a photomultiplier installed on a translation stage, or with a CCD sensor, depending on the strength of the DFG signal.

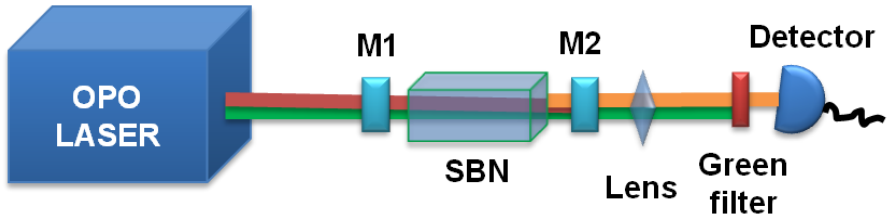

Figure 2.25: Scheme of the DFG detection of an SBN crystal.

The observations with the CCD camera show that, when the pump and the idler beams are perpendicular to the c-axis of the SBN crystal, the DFG is spread in all directions in the c-plane. The mirrors M1 and M2 shown in Figure 2.25 can be adjusted to let the pump or the idler beam or both of them be reflected back or pass through. In Figure 2.26 we display the images obtained when the crystal is illuminated by only the idler beam, only the pump beam or both at the same time. In the first case (See Figure 2.26a), a bright spot appears which has its origin in the idler beam transmitted through the crystal and with its intensity reduced by the partial filtering with a dichroic filter and by the reduced sensitivity of the CCD at that wavelength. In the second case, with only pump irradiation, the image shows a diffused background which we attribute to the luminescence in the SBN crystal (See Figure 2.26b). Finally, when both the pump and the idler irradiations are present, we observe on top of the superposition of the previous image a signal beam line on the c-plane that is created by the DFG process (See Figure 2.26c).

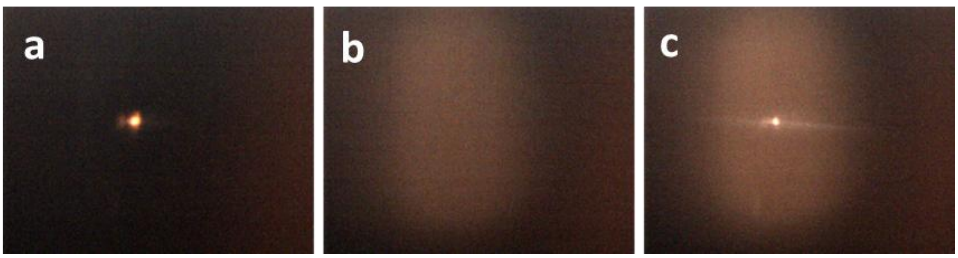

Figure 2.26: The CCD camera detection of DFG from SBN crystal at infinity when the input beam: (a) Only idler light at 1120 nm. (b) Only pump light at 532 nm. (c) Both idler light at 1120 nm and pump light at 532 nm, and the DFG signal at 1010 nm is distributed in all directions in the c-plane as a line.

With a monochromator combined with the photodiode, we have checked the signal´s wavelength. Figure 2.27 shows a wavelength scan in which both the DFG at 900 nm and the incident idler at 1300 nm appear. The intensity of the idler was strongly reduced with filters before entering the monochromator.

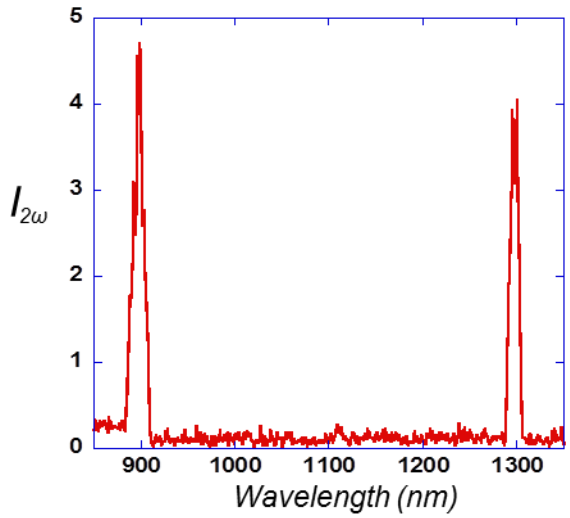

Figure 2.27: The detection of the DFG signal at wavelength 900 nm under the input pump at wavelength 532 nm and idler at wavelength 1300 nm.

An amplification of the incident idler is expected at the same time with the DFG phenomenon. However, we have detected a depletion of the infrared idler with the pump at wavelength 532 nm. We attribute this to the green induced infrared absorption (GRIIRA) [84, 85]. In order to detect the amplification of the idler, other pump and idler wavelengths

should be considered, or the GRIIRA should be reduced by high temperature operation or doping of the crystal.

2.3 Conclusions

In conclusion, we have investigated the SHG from annealed, poled, and reversely poled SBN crystals, and predicted how the poling and thermal treatments affect the random crystal structure. A second harmonic peak is observed in the direction of the fundamental beam, contributed by the crystal surface. The intensity of the SH peak generated by the random effect grows linearly with the beam path length in the structure, while that generated by the crystal surface follows the oscillation described by the Maker fringes. Besides, we also report that the DFG from the random structure has a similar spatial distribution as the SHG.

Chapter 3

SHG speckle from a transparent nonlinear random structure

As discussed in the previous chapters, scattering of light has been observed from transparent nonlinear materials where the nonlinear domains are randomly distributed in space [86]. The relatively efficient nonlinear light generation from a disordered structure has been explained with the random quasi-phase-matching condition, which is attributed to the disorder of the structure. However, no clear signs of a coherent interaction have been reported from the light generation in such nonlinear crystals. In fact, it has been shown that the coherent addition of the two interacting waves is washed out by the disorder, and the growth of the nonlinear process versus the thickness of the material becomes linear instead of quadratic [41]. In chapter 2, section 2.1.1 of the current thesis, we show that the scattering characteristics of the

SHG are not necessarily related with the disorder, indeed, a single domain could generate SHG scattered in multiple directions.

In this chapter we will present the study of SHG speckle from an SBN structure. We demonstrate that the granulation observed in the SHG pattern originates from the interference among the different SH waves independently scattered in all directions by all the nonlinear domains that compose the crystal structure. Specifically, we observe one reversely poled SBN crystal under the microscope with its surface chemically etched, so that its domain size and position distribution information is obtained. By the sum of the SHG generated from all these nonlinear domains with different sizes and positions, we simulate the angular distribution of the SH light from the whole structure. On the other hand, by measuring the angular distribution of the SH light emerging from this SBN crystal, the intensity distribution in the experiment is in very good agreement with the simulation result, both showing a speckle patterned distribution in the SHG. The theoretical model shows that a matching of the phases across the crystal among the second order nonlinear polarization and the second harmonic fields does not play a role in the reported phenomena. It is important to note that, the observation reported in this work cannot be predicted in a straightforward manner using the conventional description of SHG in SBN based on a continuous distribution of reciprocal lattice vectors [61].

This chapter contains three sections. Section 3.1 introduces the origin and properties of speckle in linear media. Section 3.2 introduces the

theoretical model of SHG speckle from a transparent nonlinear random media. Section 3.3 reports the observation and the characterization of SHG speckle from the SBN crystal, and demonstrates the validity of the theoretical simulations.

3.1 Introduction to speckle in linear media

Many of the materials present surfaces which are very rough on the scale of optical wavelengths. Such surfaces can be taken as the addition of different microscopic elements. When incident nearly monochromatic laser light is reflected from such a surface, a random interference of the light scattered from different positions within a certain range on the surface takes place, forming a speckle pattern of the reflection [87]. The spatial distribution of bright peaks and dark areas is named speckle (See Figure 3.1). The occurrence of a speckle pattern requires a coherent or partially coherent wave source and a scattering medium. If the wave source is incoherent, the speckle patterns produced by individual wavelengths have different dimensions and will normally average one another out. Speckle phenomena have been investigated for many years, but its prominent investigation began with the invention of the laser [88]. In general, the speckle pattern is a random spatial intensity distribution of light due to the interferences of many light waves of the same frequency but different amplitudes and phases.

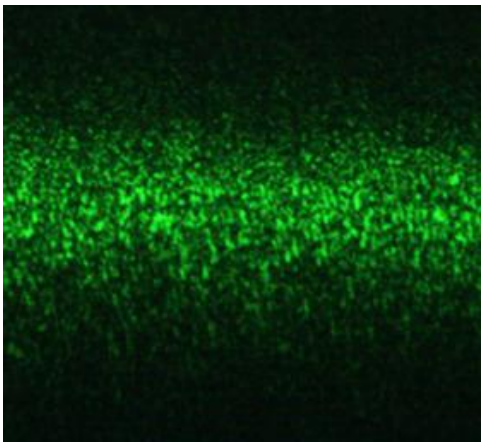

Figure 3.1: The observation of a laser speckle detected by a CCD camera.

As indicated speckle patterns arise usually when a wave-front of coherent light is reflected on a rough surface or transmitted through a medium with random variations of the refractive index. In either case, the difference in the optical path length of the light going through different points in the material produces an interference pattern at the observation point, and when its contrast is one, it is said to be fully developed. The intensity distribution in fully developed speckles follows negative exponential statistics. The probability density function is $p(I) = e^{-I/\bar{I}}/\bar{I}$, where $\bar{I}$ is the mean intensity [87, 89]. A consequence of this is that the standard deviation of the intensity equals its mean value. The optical contrast, defined as the ratio between standard deviation and mean value, is therefore unity. This happens because the path lengths of light arriving to the detection point differ in

much more than a wavelength. Thus, the phases are uniformly distributed.

Generally, depending on whether the speckle pattern changes with the observation position or not, the speckle pattern can be subjective or objective. Typically, the subjective speckle is only observed as a part of the illumination of a laser reflected from or transmitted through scattering media. In this way, the observed speckle´s characteristics depend on the imaging system, for example, the speckle pattern will change as the observer´s position changes, since the speckle is formed by the interference at the observer's retina or the camera sensor. On the other hand, the objective speckle pattern does not change with the observer´s position, which is like observing a speckle painting on the image plane. Since the speckle can be taken as the interferences of light reflected from or transmitted through different finite areas of a scattering structure, any neighboring two points in the speckle are likely to have the same intensity. However, if the two points in the speckle are far enough, their intensities can vary randomly. The minimum distinguishable distance between points in a speckle with different intensities is called the speckle size. Researchers have investigated on the space and wavelength dependence of speckle, especially, the spatial intensity correlations to characterize the average speckle sizes [90-95]. One important characteristic of speckle is that its size is inversely proportional to the diameter of the illumination laser beam. The objective speckle size follows the same principle as the subjective speckle size [88]. A typical way to characterize the average

spot size is by the autocorrelation function *R(r)* of the intensity spatial distribution *I(r)*:

$$R(r) = \frac{\int \delta I(r'+r)\delta I(r')dr'}{\int \delta I(r')^2 dr'} \tag{3.1}$$

where $\delta I(r') = I(r') - \bar{I}$.

If the incident angle changes gradually, the speckle pattern is also going to change slowly preserving part of the information of the previous speckle, which shows a memory effect of the random structure that preserves information about the angle of incidence [96, 97]. If the angular shift is small, some correlation between the speckle patterns can be found. The maximal correlation in the output speckles appears at the angle corresponding precisely to the shift in the incident angle. This happens even after multiple scattering has occurred in a linearly diffusive sample. The correlation has been observed to decrease exponentially with the variation of the incident angle in linearly diffusive samples. At the same time, the exponential factor that determines the decay has been observed to increase linearly with the thickness of the sample [96]. That is, the correlation is lost faster in thicker samples in which the light follows longer paths with more scattering events. The correlation between intensity distributions can be represented by the cross-correlation function:

$$R_{a,b}(r) = \frac{\int \delta I_a(r'+r)\delta I_b(r')dr'}{\sqrt{\int \delta I_a(r')^2 dr' \int \delta I_b(r')^2 dr'}} \tag{3.2}$$

Here, I_a and I_b represent the intensity distributions for two different speckle patterns that can be produced for different incident angles.
Besides the speckle in the linear media, researchers also have investigated on the speckle in the nonlinear light generation from random scattering media [98, 99]. However, all the reported linear and nonlinear speckles studied until the current thesis will require a scattering media with a random refractive index distribution.

3.2 Theory and simulation of SHG speckle in SBN crystal

We use the same theory to simulate the SHG from an SBN crystal which was introduced in Chapter 2 section 2.1.2, specifically, Eq. 2.6. One advantage of the theoretical formalism used here is that the effects of domain shapes and of the random distribution of domains in space can be easily separated. Moreover, it is possible to use it to make fast simulations of the SHG in this kind of structures.

We show that, for a nonlinear random structure with homogeneous refractive index, a SHG speckle appears when some degree of randomness is introduced into the polarization distribution of the domains, even if the domain size is uniform. The degree of disorder is

quantified by the parameter σ ($0 \leq \sigma \leq 1$), which measures the fraction of domains with positive polarization over the total number of domains.

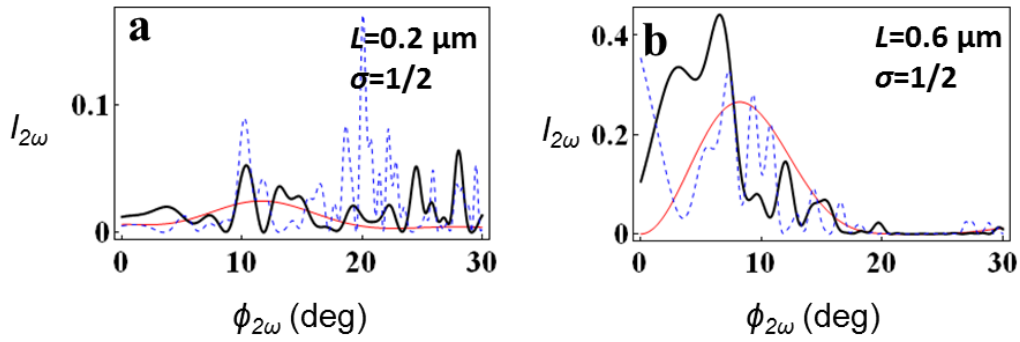

Figure 3.2: SHG speckle pattern generated from plane wave input on structures with random polarization and uniform square domain size (a) L=0.2 μm. (b) L=0.6 μm. The crystal width is 1.2 μm, and the crystal length takes the following values: 0.6 μm red, 30 μm thick black, and 60 μm dashed blue.

Figure 3.2 shows the SHG speckle pattern from a random structure, due to the interference of SHG from all domains, which are of uniform size L and antiparallel polarization. For a random structure whose width is fixed, as the structure length increases, the speckle size decreases (except in $\phi_{2\omega} = 0°$), whereas the speckle number increases. This behavior is associated with the fact that the speckle size is inversely proportional to the angular range from which the light arrives to the observation point [87]. By comparing Figure 3.2a and Figure 3.2b, one can see that if the whole structure size is fixed while the domain size L increases, the SHG becomes stronger in the forward direction.

In an SBN crystal structure after reverse poling, the ferroelectric domains have antiparallel polarization, a more or less broad distribution of sizes and can have deviations from the square shape as well as variations in the orientation. All this makes the spatial distribution of the SH intensity not follow the shape obtained from a single domain scattering, but the peaks and zeros are washed out. In this case, the SBN crystal can be modeled as a structure consisting of a group of domains with random sizes and negative polarization into a homogeneous crystal with positive polarization (See Figure 3.3). From Eq. 2.6, a structure with random position and/or polarization of the domains gives a variation of the intensity and phase with different emission angles that corresponds to a speckle pattern. Eq. 2.6 also resembles what one would obtain from a random distribution of coherent point scatterers. This leads to the prediction that the memory effect in the SHG of SBN is similar to the one obtained for linear single light scattering samples.

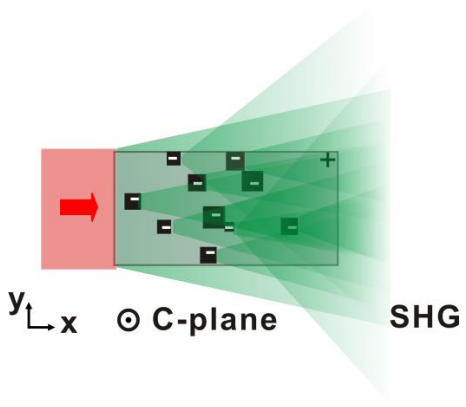

Figure 3.3: Schematic SHG from a nonlinear structure with random domain size and antiparallel polarization.

From optical microscope images of the SBN domain structure, we estimate roughly its domain size distribution in the x-y plane (See the inset of Figure 3.4). The resultant SH intensity angle distribution is plotted in Figure 3.4. From this simulation we can see that the features of the single domain size are washed out, but the average domain size determines the SHG spread angle in the c-plane [48] while the speckle remains.

The simulations also help us to better understand the origin of the speckle pattern in the SHG, and allow us to find the optimum random domain structure to generate the highest SHG intensity from SBN crystal. From Figure 2.3, the maximum intensity generated by one single domain has a periodic dependence with the size of the domain, giving a first maximum when the dimensions are close to one coherence length. The SH peaks and zeros tend to be washed out by the random distribution of sizes in one crystal. However, the SH emission can present a central maximum or some side lobes depending on the average domain size. In this way, we have predicted that the maximum SHG will happen when the domains have the average size distribution around the coherence length of SBN in the forward direction, that is about 3 μm, and when the anti-parallel ferroelectric domains are 50% in each direction [45], which is close to an SBN structure obtained after a reverse poling treatment as shown in Figure 2.24.

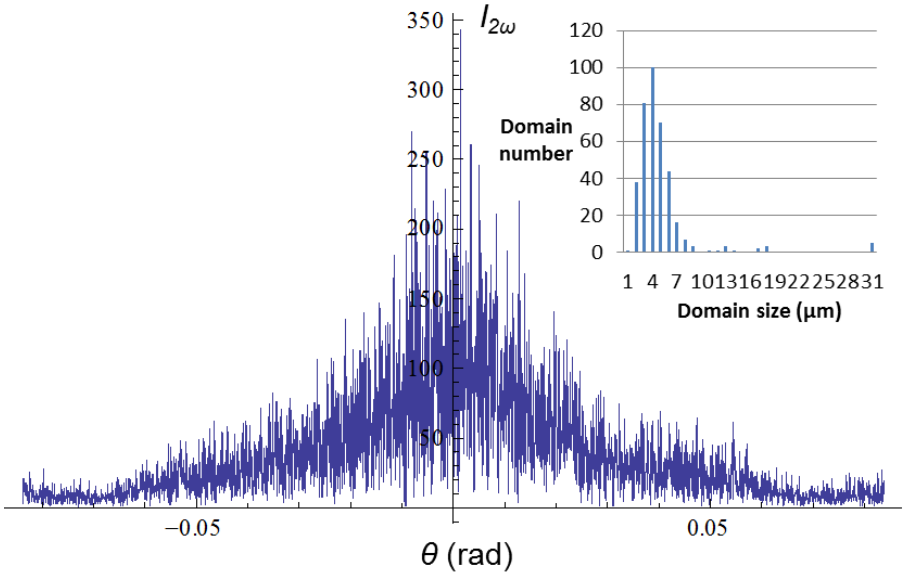

Figure 3.4: The simulated SHG intensity at different observation angles (in radians). The inset shows the domain size distribution in poled SBN crystal.

3.3 Experimental observation of SHG speckle in SBN crystal

If we measure the SHI by moving the photodiode along a line in the y direction shown in Figure 2.15, the experimental results (See Figure 3.5a) are very similar to the numerical simulation from Figure 3.4, which supports the validity of the theory. Although the linear growth of the averaged SHI with the beam path length in the crystal behaves like an incoherent addition of SHG from multiple sources, the speckle pattern demonstrates that the interference of SHG from the domains is in fact coherent.

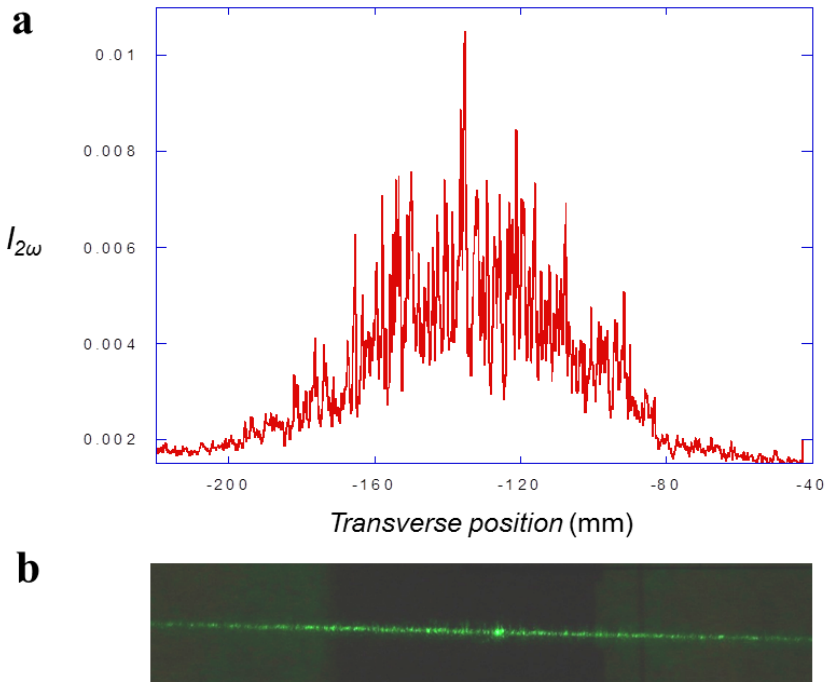

Figure 3.5: The measurement of the SHG intensity across the transverse line in the focal plane of the lens by (a) a photodiode and (b) a CCD camera.

With the same experimental set-up as in Figure 2.15, we studied the evolution of the SHG speckle pattern generated from the SBN crystal. The laser beam diameter was controlled with an iris diaphragm. The fundamental wavelength was blocked with a short pass filter before the detector. In general, we observed the SH in the far field by placing a CCD sensor in the focal plane of a lens. This configuration maps emission directions from the crystal to points on the CCD. An example of speckle pattern formed in the SH light from an SBN crystal is shown in Figure 3.6. It is possible to appreciate directly on the image that the

contrast is near unity. Moreover, the histogram of the intensity shows the negative exponential behavior.

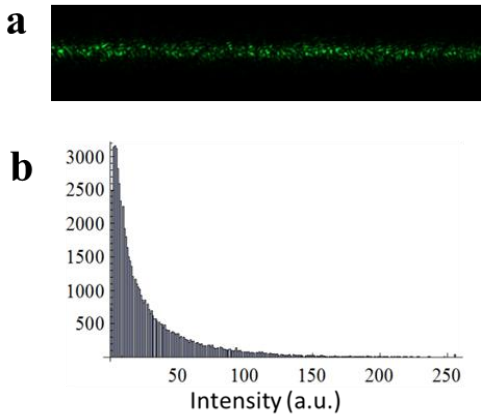

Figure 3.6: (a) Second harmonic light image created with an SBN crystal and recorded with a CCD at the focal plane of a lens. (b) Intensity histogram of the image.

Similar to the linear speckle, we find that a larger beam size or illuminating area on the SBN crystal will generate a speckle pattern with smaller speckle sizes, and vice versa (Figure 3.7). This speckle size dependence on the illuminating area is not affected by the random structure illuminated. We also observed that SBN crystals with different domain sizes will produce the same speckle size as long as the fundamental beam diameter was kept constant.

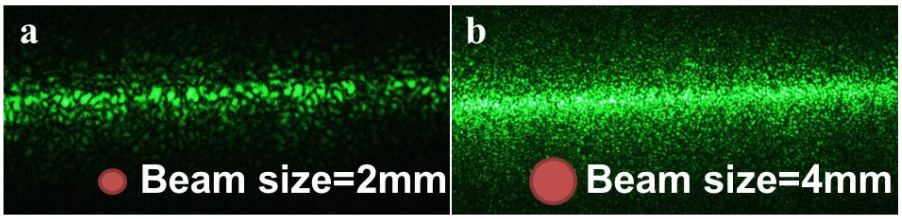

Figure 3.7: SHG speckle pattern from the same SBN crystal illuminating with different beam diameters (a) 2 mm (b) 4 mm.

To characterize the average spot size, we substitute the integrals in Eq. 3.1 by discrete sums over CCD pixel readings. In Figure 3.8 we show how the autocorrelation length of the SH speckle formed in front of the crystal is increased as the diameter of the fundamental beam decreases. On the other hand, measurements from samples with different domain sizes gave the same autocorrelation as long as the beam diameter was kept constant. This is a common feature of speckle patterns which are independent on the details of the microstructure.

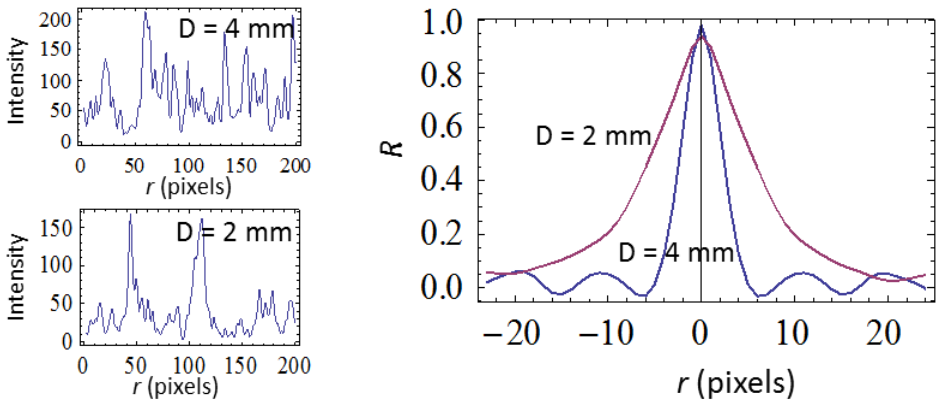

Figure 3.8: Left: speckle profiles formed with fundamental beam diameter of 4 mm and 2 mm. Right: autocorrelation function of the speckle profiles.

With Eq. 3.2, to measure the memory effect in the SH speckle from our transparent crystal, we recorded the intensity patterns while the crystal was rotated at angle θ around one axis perpendicular to the plane of incidence. The fundamental beam and the CCD camera used for detection remained stationary. Thus, the maximum correlation is obtained for r=0. The maximum correlation as a function of the rotation angle θ for a 5 mm thick crystal is shown in Figure 3.9.

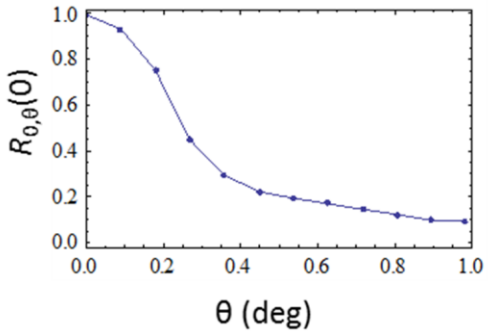

Figure 3.9: Correlation of the SH intensity spatial distribution as a function of the incident angle θ.

If we compare with the results obtained for different thickness of diffusive materials in reference [96] we observe that the correlation decay with the angle in our experiment is on the same order as the correlation decay in ground glass samples (0 thickness). This indicates that the SH scattering from a transparent material like SBN is similar to the linear single light scattering. The large memory effect in this kind

of SH scattering can be relevant in the spatial control of the light that we will discuss in chapter 4.

3.4 Conclusions

In this chapter, we have demonstrated, both experimentally and theoretically, second-harmonic speckle pattern formation by a transparent SBN crystal. Due to the lack of light scattering in the linear regime, these findings represent a novel interpretation of the manifestation of coherent optical phenomena occurring in random nonlinear optical materials. Experimentally, the SHG speckle pattern generated by a transparent SBN crystal is measured for different diameters of the fundamental beam. By using a theoretical Green's function formalism, the reported speckle observations are explained as a result of the linear interference among the second-harmonic waves generated in all directions by each of the nonlinear domains forming the nonlinear crystal. Different from the previous description of SHG in SBN based on a continuous distribution of reciprocal lattice vectors, this intuitive explanation demonstrates the nonlinear speckle generation from the random structure in a straightforward way.

Chapter 4

Control of the SHG from SBN crystal by wave-front phase modulation

The SHG speckle obtained in SBN crystal spans a wide range of emission directions, which greatly reduces its efficiency in one particular direction. In this chapter we demonstrate a wave-front phase modulation method to focus the SHG from an SBN crystal from many speckles to a single point [46]. Such approach is based on a concept similar to the one used to focus the fundamental beam through a strongly scattering turbid media [35]. In essence, it consists on a feedback optimization algorithm used to shape the fundamental beam by controlling the phase corresponding to each segment of a spatial light modulator (SLM).

This chapter contains three sections. Section 4.1 introduces the wave-front shaping method as used in linear light transmission experiments.

Section 4.2 presents the experimental control of SHG light with a SLM by the wave-front shaping method. We show the results for the focusing of the SHG speckle from a transparent SBN crystal with a random distribution of antiparallel domains. Section 4.3 develops a theoretical model for the SHG spatial control. The SLM effect is modeled by modulation of the phases of the incident beam that affect different regions of the crystal. The light concentration efficiency at different emission angles is calculated.

4.1 Introduction to the wave-front shaping method

When a beam of light interacts with a homogeneous medium, the light follows a well-defined path. However, as presented in chapter 3, if this light interacts with an inhomogeneous material such as a thin layer of powder, the light will be scattered by the random distribution of particles, and it will produce a speckle pattern with dark and bright spots when the scattered light paths interfere with each other. This phenomenon can be problematic for optical imaging, spectroscopy and telecommunication. For example, when we want to observe the structure inside the human body, or communicate with the satellite with laser during a cloudy day, etc.

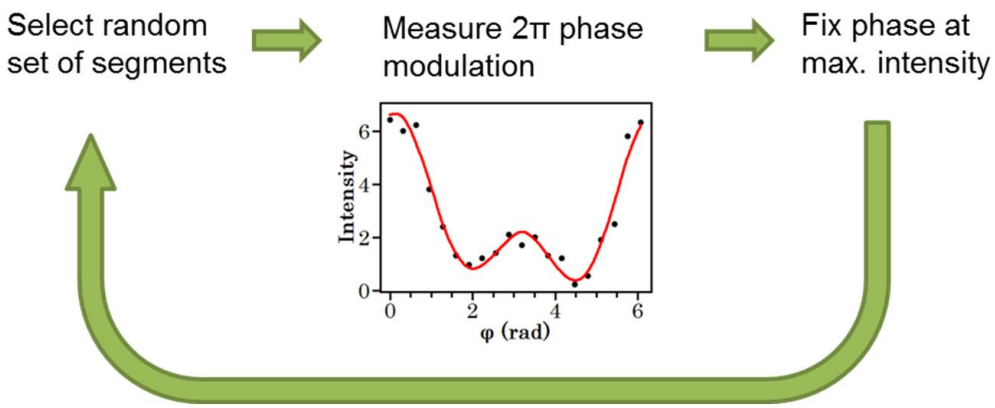

Figure 4.1: Schematic of the optimization algorithm used to focus the light at the intended point or area by the wave-front phase modulation method. The inset is the evolution of second harmonic intensity as the phase is modulated from 0 to 2π.

Researchers have investigated on the control of light transmission through strongly scattering media both in space and time by different methods: taking advantage of the time reversal symmetry [36, 100] with the phase conjugation method [101, 102], measuring and making use of the random transmission matrix [103-106], which relates the free modes of the input and output of light, or implementing feedback optimization algorithms [107, 108]. The potential for applications is large: Opaque lens super-focusing beyond the diffraction limit [109-115]; Optimal light transmission through turbid media [116-119]; Better imaging in biological tissues [34, 120]; Operation control of a random laser [121], etc. For all these technologies and applications, it is convenient to use an SLM to shape the wave-front, usually under the operation of a liquid crystal display [122, 123].

The goal of the wave-front shaping method is to replace a plane wave incidence by placing a “phase mask” on the plane wave in such a way that the wave-front arriving at the random material has a modulation on its phase and a different light interference pattern is formed after the material. According to the work done by Vellekoop, etc [124], a feedback algorithm is designed to control the SLM to realize the optimized SH focus at the intended place. A schematic of the optimization algorithm used to get the maximum light intensity at the intended point or area is illustrated in Figure 4.1. The light transmission is detected by a CCD camera (or a photo diode). The CCD camera sends the detected image to a computer, the computer reads the image information, and tells the SLM to modulate the phase of the beam until the desired image is obtained by the detector.

In this way, instead of getting a speckle with bright and dark spots, one single bright spot can be obtained after an opaque material. Moreover, the focus can be much smaller than the focus obtained by a regular lens, since it overcomes the diffraction limit of the latter case [110, 113]. This method to focus or modulate light through opaque material is very simple and highly interesting in the fields of microscopy, nano-surgery, and astronomy, etc.

4.2 Experimental control of SHG from SBN crystal using a spatial light modulator

In general, phase control of the incident wave-front by means of phase only SLMs [35, 105] is based on the linearity of the transmission matrix. The complex coefficients of the transmission matrix t_{oi} connect the optical field at points in a surface containing the sources (input modes E_i) with the optical field at points in the detection surface (output modes E_o) through the equation:

$$E_o = \sum_i t_{oi} E_i \tag{4.1}$$

With an independent control of the phase of all input modes one can transform the sum in Eq. 4.1 in a sum over real numbers in such a way that the output intensity in one mode is maximized.

In the case of three wave mixing, the transmission matrix needs to be replaced by a third rank tensor t_{oij} relating the output modes at the resulting frequency with combinations of input modes from the incident beams E_{iA} and E_{jB} in the following way:

$$E_o = \sum_{i \in A} \sum_{j \in B} t_{oij} E_{iA} E_{jB} \tag{4.2}$$

For sum-frequency, difference-frequency or two beam SHG we can control the phase of the input modes in one group, A or B, keeping the other group input fixed. Eq. 4.2 can then be reduced to a single sum like Eq. 4.1 by including the constant E field inside the transmission matrix. On the other hand, if we consider a process like SHG from one fundamental beam, the input modes E_{iA} and E_{jB} belong to the same set (A=B) and are therefore modified at the same time. In this case, the crossed terms in the double summation may always have different phases for any combination of input phases. Yet, an optimization method could still find a combination of input phases that leads to the concentration of the generated intensity in an output mode.

In the optimization methods for linear light transmission, the phase of one or several input modes is modulated from 0 to 2π while the rest of the modes are kept fixed. This produces an intensity modulation of the form $I = {a_1}^2 + {a_2}^2 + 2a_1a_2\cos(\varphi - \phi)$ where a_1 and φ are, respectively, the amplitude and phase of the modulated modes together with their respective transmission matrix elements and a_2 and ϕ correspond to the amplitude and phase of the fixed modes with their matrix elements. After the measurement, the modulated phase is fixed at $\varphi = \phi$ corresponding to the maximum intensity. This step is repeated multiple times changing each time the modes that are modulated.

When the process is applied to SHG the intensity follows a different dependence with the modulated phase. In a similar way as explained above for the linear case, we can reduce the modes in Eq. 4.2 into two

groups: one that includes all terms whose phase is modulated by φ, and the second for the fixed part. Eq. 4.2 is then rewritten as

$$E_o = a_{o11}e^{i(\phi_{o11}+2\varphi)} + a_{o22}e^{i\phi_{o22}} + a_{o12}e^{i(\phi_{o12}+\varphi)} \tag{4.3}$$

where we have also separated explicitly the amplitude and phase for each term in the sum, where a_{o11} and ϕ_{o11} are, respectively, the amplitude and phase of the modulated modes together with their respective transmission matrix elements, and a_{o22} and ϕ_{o22} correspond to the amplitude and phase of the fixed modes with their matrix elements, and a_{o12} and ϕ_{o12} are the amplitude and phase of the cross terms from both the modulated and fixed modes. The intensity of the output mode resulting from it has the form

$$\begin{aligned} I = {a_{o11}}^2 + {a_{o22}}^2 + {a_{o12}}^2 + 2a_{o11}a_{o22}\,cos(2\varphi + \phi_1 - \phi_2) \\ + 2a_{o11}a_{o12}\,cos(\varphi + \phi_1) \\ + 2a_{o22}a_{o12}\,cos(\varphi - \phi_2) \end{aligned} \tag{4.4}$$

where we have rewritten $\phi_1 = \phi_{o11} - \phi_{o12}$ and $\phi_2 = \phi_{o22} - \phi_{o12}$. This function can have two local maxima in the interval of φ between 0 and 2π. We always selected the higher of the two local maxima during the optimization process.

As in the work presented in the rest of this thesis, the nonlinear material used in the experiments was an SBN crystal. To maximize the SHG

efficiency, the crystal was poled at room temperature under a 400 V/mm electric field along the crystallographic c-axis with alternation of the field polarization during at least two cycles. The resulting domain structure consists of a random pattern of needle shaped antiparallel domains with an average width on the order of 3 μm. This is close to the coherent length of the SHG process in the collinear configuration and, when the fundamental beam propagates perpendicular to the c-axis, it yields a stronger intensity in directions on the plane perpendicular to the crystal c-axis within 20° from the propagation direction of the fundamental beam. The SHG is scattered in the mentioned directions forming a speckle pattern.

The experimental setup is shown in Figure 4.2. We used a Q-switched Nd-YAG laser emitting 6 ns pulses at 10 Hz repetition rate and 1064 nm wavelength. The laser beam was expanded before arriving to the Liquid-Crystal-on-Silicon SLM (LCoS model X10468-03 from Hamamatsu). Each pixel of the SLM corresponds to one segment of the incident beam, and each pixel´s gray value decides the corresponding incident beam segment´s phase. In this way, we divide the input beam wave-front into a certain number of small equal segments, and the phase of each segment can be controlled respectively by the phase only SLM. The modulated beam was then reduced using a 4f system in such a way that the image of the SLM was projected on the nonlinear crystal. The transmitted light at the fundamental wavelength was then removed using a short pass filter. The detection of the SHG at 532 nm was made at the far field using a CCD sensor at the focal plane of a lens.

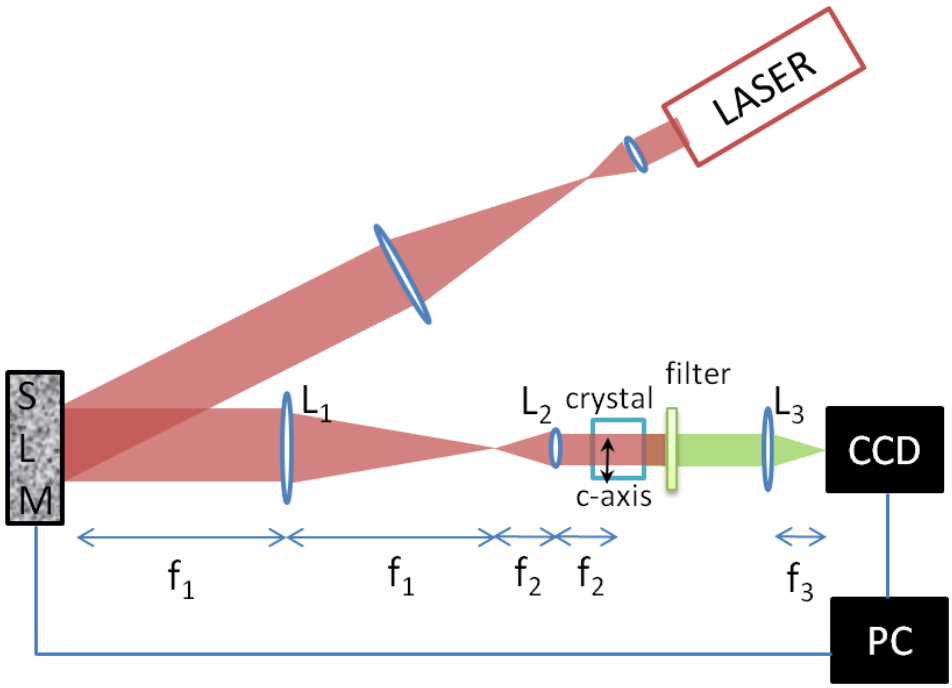

Figure 4.2: Experimental setup to focus the SHG from an SBN crystal by shaping the wave-front of the incident beam with a SLM. The inset is a schematic of the SH light focused through the SBN crystal under phase modulated incident beam.

Several optimization algorithms have been tested by others for focusing light transmitted through diffusive media [107]. In general, they are able to find solutions such that a maximum possible intensity is achieved at the selected point. However, in the case of SHG, it is not possible to be certain that the global maximum would be found following such procedure because the crossed terms in the double sum may provide several local maxima. We have used the partitioning algorithm, which has been shown to provide the fastest growth in the intensity for linear light transmission. This method modifies the phases of half of the segments of the wave-front each time instead of one by

one, improving the signal to noise ratio in the measurement. The final efficiency of this method is similar to the other methods [107]. The SLM pixels are randomly divided into two equal sized groups, keeping one group fixed and adding to the pixels on the other group a phase that is modulated continuously from 0 to 2π while the intensity of the SHG at the desired direction is recorded. The image of the SHG in the area chosen for optimization is taken as a feedback signal to control the phases of the SLM segments. We detect for which phase the maximum intensity occurs and we fix the phase of the pixels at that value. The process is iterated many times changing randomly the set of pixels whose phase is altered. The data acquisition and phase control are both realized by a LABVIEW program. We found that this method is able to provide a good enhancement of the intensity at the selected point.

Because of the quadratic dependence of the SH light with the fundamental light intensity, in some cases the optimization process can lead to the focusing of the fundamental light in the crystal. In general, the intensity at any detection point can be increased just by focusing the fundamental light in the crystal. If this is not taken into account, the optimization algorithm can configure the SLM as a sort of kinoform lens. The effect is an overall increase of the intensity and a growth in the speckle size because of the smaller illuminated area. The result is an overall higher second harmonic intensity but no light concentration in one direction. One way to avoid that is to place the crystal at the image plane of the SLM. At that plane, there will be no variations in the intensity for any phase pattern of the SLM. Another possibility is to take for optimization the intensity ratio between the desired point and a

wide reference area around it in such a way that the intensity will grow only in one point and not everywhere. The reference measurement has the additional advantage of reducing the noise introduced by pulse to pulse intensity fluctuations.

For example, if there is no such a 4f lens system in the experimental setup as in Figure 4.2, in the optimized phase pattern of the SLM, it is possible to appreciate a circular symmetry that is causing the focusing effect. The fundamental beam is concentrated in the crystal as a result of the optimization process (Figure 4.3), and the resulting SH distribution presents the same angular dispersion but larger and higher intensity speckles. The increase in the size of the speckles can be understood by the smaller illuminated area, as explained in chapter 3.

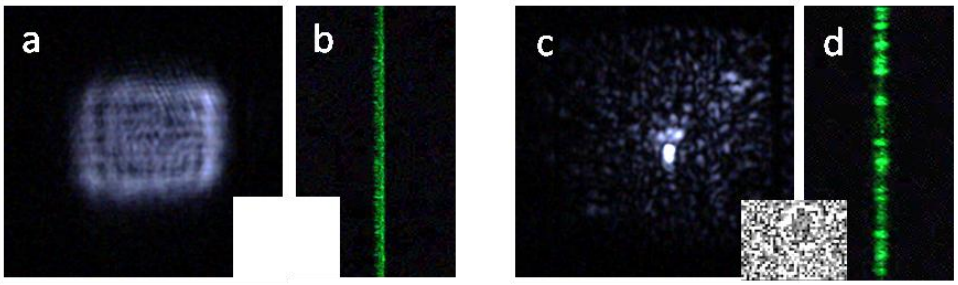

Figure 4.3: (a) Image of the fundamental beam in the crystal with homogenous phase pattern in the SLM and (b) corresponding SH intensity at the far field. (c) Image of the fundamental beam in the crystal after an optimization process and (d) corresponding SH intensity at the far field. The insets are greyscale representations of the phase pattern at the SLM.

In general, we would like to increase the intensity in one spot and remove the rest of the speckle. Moreover, the uncontrolled focusing of light in the sample can produce optical damage. To prevent this, we use a configuration in which the image of the SLM is projected on the crystal. With such an experimental setup as in Figure 4.2 with f1 = 500 mm, f2 = 50 mm, and f3 = 150 mm, and dividing the SLM in a 30×40 matrix we obtained the results displayed in Figure 4.4. The original SLM dimensions of 12 mm × 16 mm were reduced by the 4f system to 1.2 mm × 1.6 mm at the central position of the crystal. The crystal length was 5 mm, which makes the intensity homogeneity at the crystal to be only approximate. In our experiment, the optimization process took about 50 minutes to reach a ratio of nearly 700, between the intensity at the selected point and the average intensity at the areas around it. At each step 20 measurements with different phases were taken, and the phase φ was set at the value corresponding to the maximum intensity. Around 1500 iterations were necessary to reach the saturation value of the intensity. The results are close to the ones obtained for linear light diffusion [12]. The enhancement is on the same order as the number of modulated pixels in the SLM and it takes about the same number of iterations to reach it.

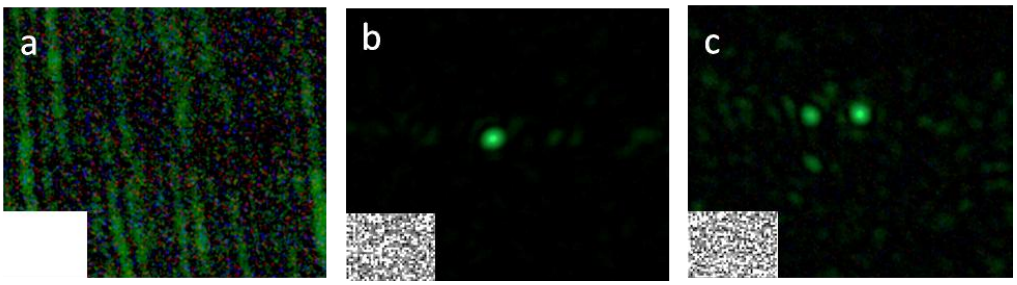

Figure 4.4: (a) SH intensity with a homogeneous phase pattern in the SLM, (b) after the optimization of the intensity at one point, and (c) after the optimization of the intensity at three points. The brightness scale of the image on (a) is increased with respect to (b) and (c). The insets are greyscale representations of the phase pattern at the SLM.

The stability of the crystal structure allows maintaining the optimized emission during long periods of time without changing the phase pattern in the SLM. The enhanced spot was still observed without appreciable loss in intensity when the stored optimized wave-front was displayed again in the SLM six days after the optimization process.

It is possible to enhance the intensity of several points at the same time by optimizing their sum (Figure 4.4c). However, with the used algorithm, it is difficult to get an even intensity in all of them as already noted in reference [107]. The use of different algorithms or the measurement of the transmission tensor [105] could bring the possibility of forming images in the emitted light.

The broadband SHG characteristic of the random structure allows the simultaneous frequency doubling or mixing of different wavelengths in the same sample. The optimization of different processes would

probably require a phase pattern change in the SLM. In any case, the possibility of red, green, and blue emission through frequency doubling or mixing of infrared lasers in the same crystal [125], together with beam shape controlled by the wave-front modulation as demonstrated here, could find some applications for example in laser display technology.

4.3 Theory of controlling SHG from SBN crystal by phase modulation method

In this section, we present a detailed theoretical study of the spatial intensity control of SHG by fundamental beam wave-front modulation. We consider a crystal structure characterized by a homogeneous refractive index but featuring random changes in the second order nonlinear susceptibility. More specifically, we focus our discussion in a structure similar to the one that can be found in ferroelectric crystals such as SBN or $LiNbO_3$. In such crystals, long domains are formed along the crystallographic c-axis with antiparallel orientation. In the case of SBN, the size and position of the domains are usually randomly distributed. A random distribution can also be introduced in $LiNbO_3$ by electric field poling with designed patterns.

Our theoretical framework is based on a generalization of a first principle Green function formalism, able to account for the effect introduced by the spatial light modulation of the fundamental beam.

The spatial light modulation is modeled by dividing the structure into N segments along the crystal width L_y, and applying to them a fundamental wave with variable phases. We have found the phase front configurations that lead to an optimized SHG, and the effectiveness in the optimization of the SHI from a nonlinear random structure is affected by the target direction. Our numerical results show how the second-harmonic light is influenced by both the disorder in the structure and the boundaries of the crystal. Particularly, we find that the net result from the interplay between disorder and boundary effects is strongly dependent on the dimensions of the crystal and the observation direction. Remarkably, our calculations also show that, although in general the maximum possible enhancement of the second order light is the same as the one corresponding to linear light scattering in turbid media, in the Cerenkov phase-matching direction the enhancement can exceed the linear limit.

Without loss of generality, and in order to simplify the theoretical discussion, we restrict our analysis to the two-dimensional (2D) plane perpendicular to the c-axis. Since both fundamental and SHG light propagate along that plane, no fundamental difference is expected for a full three-dimensional (3D) treatment. We describe the plane with x-y Cartesian coordinates. We take x as the fundamental beam propagation direction. The phase of the fundamental beam is modulated along the perpendicular direction (y). Specifically, the beam is divided into N segments, and the phase of each segment φ_n ($1 \leq n \leq N$) is modulated independently between 0 and 2π. If we assume the fundamental beam is perfectly collimated, and by neglecting the effect of beam diffraction

during propagation within the crystal, the SH signal generated by the mix of the fundamental beam from two different phase segments can be neglected. This allows increasing the computational efficiency of our theoretical treatment, as we need to consider only the SH generated from each segment separately.

Within the Green function formalism, the SHG electric amplitude $E^{2\omega}$ from one single domain with dimensions L_x and L_y along the x and y directions, respectively, and located at position (x,y) can be expressed as in Eq. 2.1 [48]. Once the SH electric field from a single domain has been calculated, the SH electric field from the whole structure can be obtained as the result of the interference of the SHG from each domain. In this calculation we found it convenient to divide the structure into N groups corresponding to the segments whose phases are modulated. Thus, if we assume that there are M domains in each of the N groups modulated by phases φ_n ($1 \leq n \leq N$) (Figure 4.5), (x_{mn}, y_{mn}) is the position of the m^{th} domain in the n^{th} group, which can be described as domain mn, and the SHG electric amplitude from this domain is $E^{2\omega}_{x_{mn},y_{mn}}$, we can write:

$$E^{2\omega} = \sum_{n=1}^{N} \sum_{m=1}^{M} E^{2\omega}_{x_{mn},y_{mn}} e^{i2\varphi_n} \tag{4.5}$$

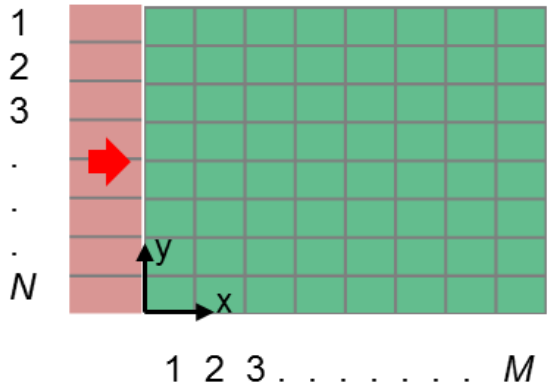

Figure 4.5: Schematic of a structure divided into N groups of phase modulation segments, with M domains in each group.

In the crystal structure considered, the absolute value of the effective nonlinear susceptibility is constant, while only its sign changes for domains with opposite polarization. We take P_{mn} as the sign given by the polarization of domain *mn*, and the value of P_{mn} is 1 for domains of positive polarization, and -1 for domains of negative polarization. From Eqs. 2.1 and 4.5, the SHI can be expressed as:

$$I^{2\omega} = d\left|\sum_{n=1}^{N}\sum_{m=1}^{M} P_{mn}\, L_{x_{mn}} L_{y_{mn}} e^{i(x_{mn}\Delta k_x + y_{mn}\Delta k_y)} sinc\left(\frac{\Delta k_x L_{x_{mn}}}{2}\right) sinc\left(\frac{\Delta k_y L_{y_{mn}}}{2}\right)\right. \tag{4.6}$$

With the appropriate values for φ_n, the contributions from the N modulated groups can be added in phase. The maximum SHI occurs when the modulated phases φ_n compensate the phases introduced by the rest of the terms. We define the maximum SHI achieved by the phase

modulation is $I_{2\omega}(\varphi_n)_{max}$, and the SHI under plane wave input is $I_{2\omega}(\varphi_n=0)$. Thus, the SHG enhancement efficiency η is the proportion between $I_{2\omega}(\varphi_n)_{max}$ and $I_{2\omega}(\varphi_n=0)$, that is, $\eta = I_{2\omega}(\varphi_n)_{max} / I_{2\omega}(\varphi_n=0)$.**

4.3.1 Control SHG from a homogeneous crystal

Firstly, we consider the structure case of a rectangular homogeneous crystal, from which the SHG is maximized for a certain angle. The length of the crystal is L_x and the width is L_y. The input beam is divided into N segments, the width of each segment is L ($L=L_y/N$), and the segment phases are modulated by φ_n ($1 \leq n \leq N$). The polarization sign P_{mn} takes the value 1, so the SHI from this homogeneous crystal is expressed as:

$$I_{2\omega} = d\left(L_x L sinc\left(\frac{\Delta k_x L_x}{2}\right) sinc\left(\frac{\Delta k_y L}{2}\right)\right)^2 \left|\sum_{n=1}^{N} e^{inL\Delta k_y} e^{i2\varphi_n}\right|^2 \qquad (4.7)$$

If we introduce a phase modulation in such a way that φ_n compensates the phase from $nL\Delta k_y$, so the maximum SHI achieved by the phase modulation $I_{2\omega}(\varphi_n)_{max}$ is proportional to N^2L^2. From Eq. 4.7, $I_{2\omega}(\varphi_n)_{max}$ features a quadratic growth with the crystal width $L_y = NL$, while it has the same relation with the crystal length L_x as the $I_{2\omega}$ under the plane wave input, as shown in Figure 2.3 in chapter 2. On the other hand, the SHI under plane wave input $I_{2\omega}(\varphi_n=0)$ is obtained when $\varphi_n = 0$ for all n.

Thus, from Eq. 4.7, the SHG enhancement efficiency is deducted as $\eta = N^2/\left|\sum_{n=1}^{N} e^{inL\Delta k_y}\right|^2$.

For the collinear case, Δk_y=0, so $\eta(\phi_{2\omega}$=0°)=1. Therefore, $I_{2\omega}$ in the beam propagation direction cannot be optimized through this phase modulation method. For other angles, the precise value of the enhancement depends on the size of the modulated segments L. If $L = 2\pi/\Delta k_y$, the denominator in the expression for η is N^2 and thus η =1 (no enhancement). In contrast, if the wave-front modulation is performed using small segments ($L << \pi/\Delta k_y$) the denominator in η can be approximated by $\left|\int_0^N e^{in} dn\right|^2 = 2 - 2\cos N$. This term corresponds to the effect of the crystal width (in this case proportional to N) on the intensity under plane wave irradiation. The oscillation in the denominator is translated into an oscillation in η. The minima in the oscillation correspond to $\eta = N^2/4$, that features a quadratic growth with N. Note also that the possible zeros in the denominator make that η can diverge to infinity for certain values of N. However, this divergence, that has its origin in zero intensity under plane wave for the corresponding crystal width, does not lead to an infinite value in the maximized intensity. An example of the SHI from a homogeneous crystal optimized in the collinear angle, the Cerenkov angle, and an angle at which neither Δk_x nor Δk_y is 0 is given in Figure 4.6.

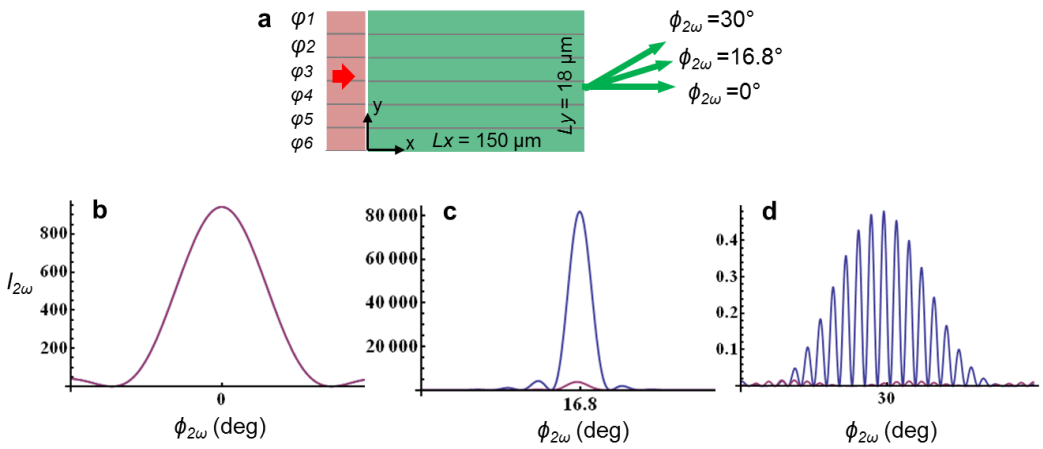

Figure 4.6: (a) Schematic of the SHG in a homogeneous structure of 18 μm wide and 150 μm long, and the phases of the incident beam are divided into N=6 modulation segments. The SHI is optimized at (b) $\phi_{2\omega}$=0°, (c) $\phi_{2\omega}$=16.8°, (d) $\phi_{2\omega}$=30°. Red line: SHI under plane wave. Blue line : SHI optimized by phase modulation.

4.3.2 Control SHG from a random distribution of domains

Now we consider the SHI from a random distribution of square domains with positive polarization. Each of the domains is with random size from 0 to L μm, and is randomly located at (x_{mn}, y_{mn}), while x_{mn} randomly takes the value between 0 and ML μm, and y_{mn} between 0 and NL μm (Figure 4.7). Due to the randomness of the polarization, the $I_{2\omega}$ under both plane wave and phase modulated incidence will grow linearly with M (Figure 4.8) [44].

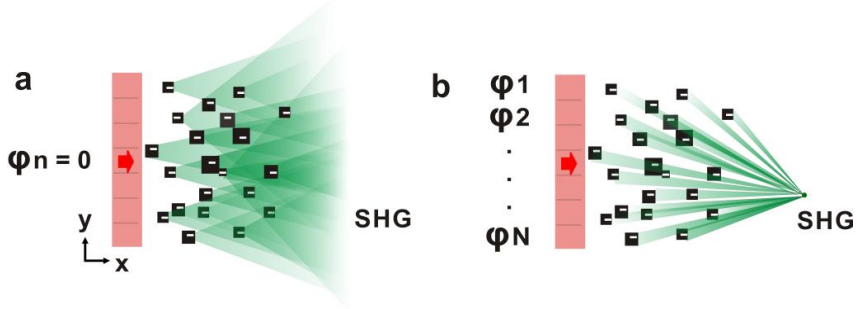

Figure 4.7: Schematic of SHG from a group of random domains with negative polarization: (a) SHG under plane wave incidence. (b) SHG optimized at one point by wave-front modulation.

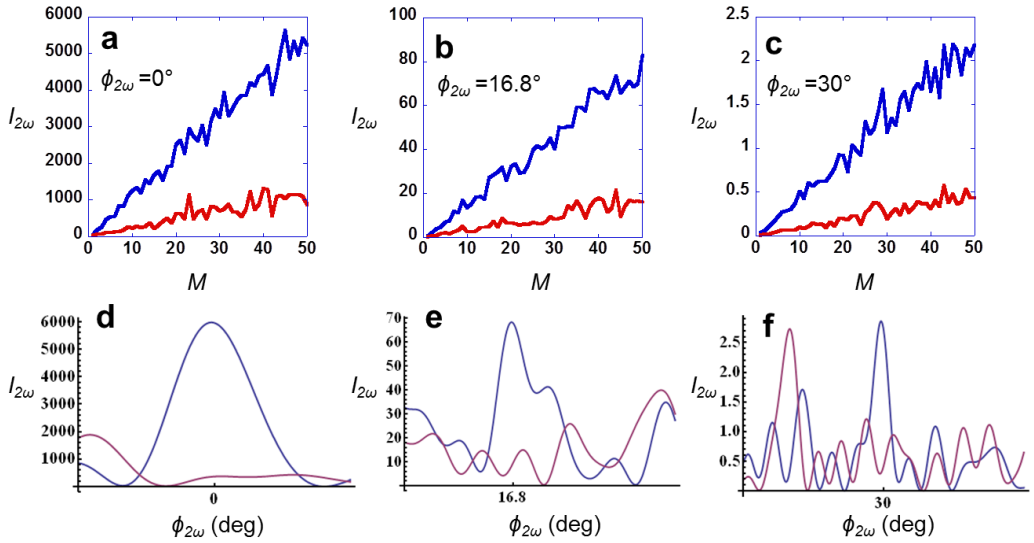

Figure 4.8: The SHI growth with the number of domains in each phase segment (M), when SHI is optimized at (a) $\phi_{2\omega}$=0°, (b) $\phi_{2\omega}$=16.8°, and (c) $\phi_{2\omega}$=30°. The lower row of plots represents the SHI angular distribution from a structure of 6*50 domains when SHI is optimized at (d) $\phi_{2\omega}$=0°, (e) $\phi_{2\omega}$=16.8°, and (f) $\phi_{2\omega}$=30°. The structure is made of domains of positive polarization, random sizes between 0 and 3 μm and random positions, and the phase segment number is N=6. Red line: SHI under plane wave, and blue line: SHI optimized by phase modulation.

However, the growth with N under the plane wave input will be linear while under phase modulation optimization can be quadratic (Figure 4.9). As a result, the maximum SHG intensity enhancement by phase modulation is $\eta=N$.

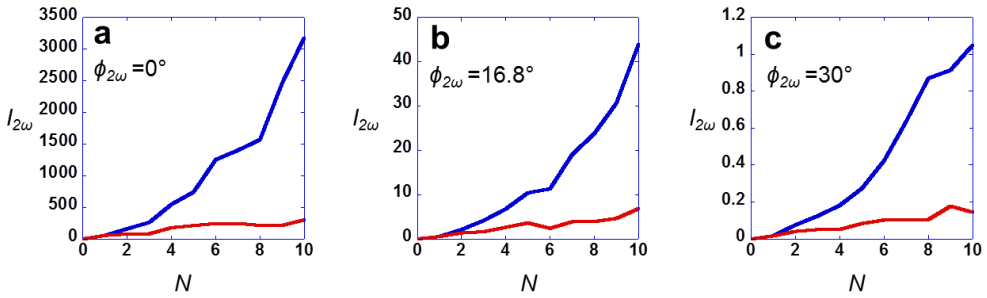

Figure 4.9: The SHI growth with the phase segment number (N), when SHI is optimized at: (a) $\phi_{2\omega}$=0°, (b) $\phi_{2\omega}$=16.8°, and (c) $\phi_{2\omega}$=30°. The structure is made of domains of positive polarization, random sizes between 0 and 3 μm and random positions, and the domain number in each phase segment is M=10. Red line: SHI under plane wave, and blue line: SHI optimized by phase modulation.

4.3.3 Control SHG from a random crystal structure

We further introduce the nonlinearity in the spaces between the random distribution of domains considered in the previous section, together with a uniform crystal boundary. In this case, the modeled structure consists of a group of domains with random sizes and negative polarization into a homogeneous rectangular crystal with positive polarization, whose width is L_y and length is L_x (See Figure 4.10). We still assume the domains are square-shaped, and the side length of the domain mn is L_{mn}, where L_{mn} takes random values from 0 to L. L

corresponds to the width of each phase segment along the y direction, so that the domain position x_{mn} will take random values between L_{mn} and L_x, and y_{mn} between $(n\text{-}1)L+L_{mn}$ and nL. In our simulations the eventual spatial overlap of two domains was not prevented. However, comparing the results with those obtained in simulations of constant sized domains, for which there is no overlap, we conclude that the eventual overlap of domains does not affect the main conclusions presented here.

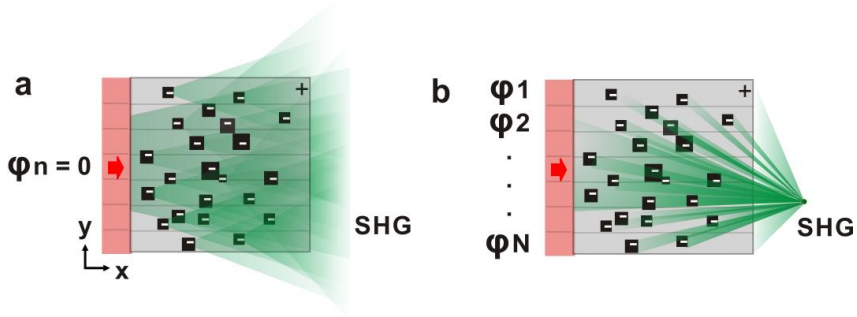

Figure 4.10: Schematic of SHG from a nonlinear structure with random domain size and antiparallel polarization: (a) SHG under plane wave incidence. (b) SHG optimized at one point by wave-front modulation.

We still define σ as the proportion of the area covered by domains with polarization pointing up (P = 1) to the total structure area. From Eq. 4.6, we compute the SHG before and after optimization for three representative directions, namely, in the collinear angle, the Cerenkov angle, and an angle at which neither Δk_x nor Δk_y is 0. We find the growth of the SHI in the random crystal structure can show properties of that from a homogeneous crystal and that from a group of random

domains, depending on the randomness of the structure. If σ takes the value 1/2, the SHG from the structure shows the random property (Figure 4.11). However, if σ is a number between 0 and 1 but not 1/2, the SHG from the structure is likely to show the property of that from a homogeneous crystal (Figure 4.12).

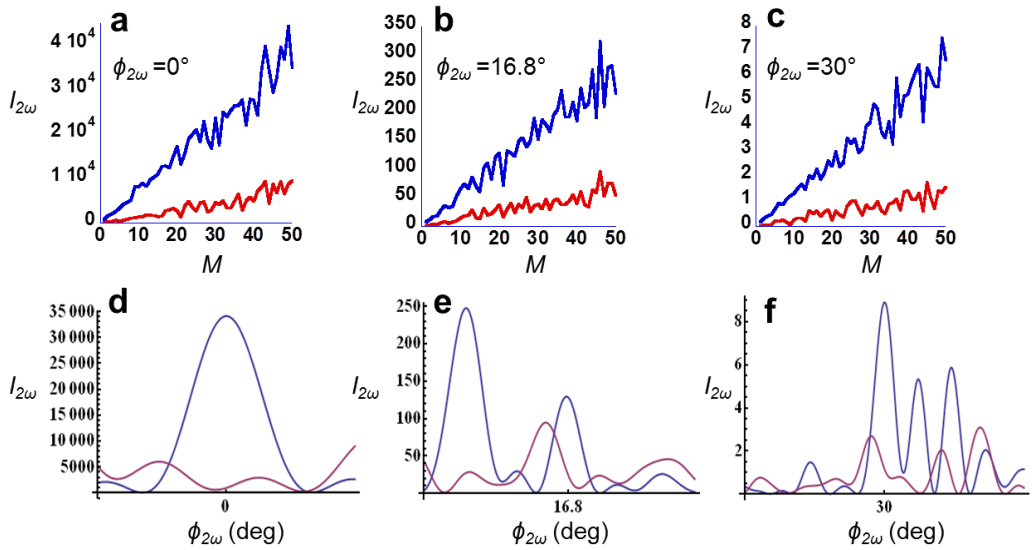

Figure 4.11: The SHI growth with *M*, the number of domains in each phase segment, when SHI is optimized at (a) $\phi_{2\omega}$=0°. (b) $\phi_{2\omega}$=16.8°. (c) $\phi_{2\omega}$=30°, respectively. The SHI angle distribution from a structure of 6*50 domains before and after the optimization at (d) $\phi_{2\omega}$=0°, (e) $\phi_{2\omega}$=16.8°, (f) $\phi_{2\omega}$=30°. The structure is made of uniform domain size 3 μm and random polarization (σ=1/2), and the phase segment number *N*=6. Red line: SHI under plane wave, and blue line: SHI optimized by phase modulation.

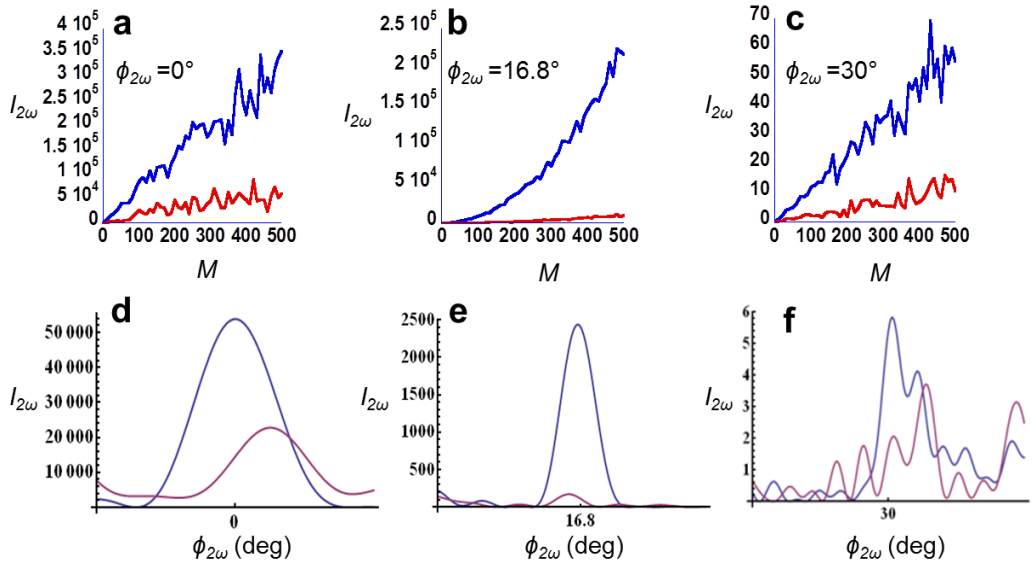

Figure 4.12: The SHI growth with *M*, the number of domains in each phase segment, when SHI is optimized at (a) $\phi_{2\omega}$=0°. (b) $\phi_{2\omega}$=16.8°. (c) $\phi_{2\omega}$=30°, respectively. The SHI angle distribution from a structure of 6*50 domains before and after the optimization at (d) $\phi_{2\omega}$=0°, (e) $\phi_{2\omega}$=16.8°, (f) $\phi_{2\omega}$=30°. The structure is made of uniform domain size 3 μm and random polarization (σ=2/3), and the phase segment number *N*=6. Red line: SHI under plane wave, and blue line: SHI optimized by phase modulation.

If we define

$$t_n = \sum_{m=1}^{M} P_{mn} L_{mn}^2 \, sinc\left(\frac{\Delta k_x L_{mn}}{2}\right) sinc\left(\frac{\Delta k_y L_{mn}}{2}\right) e^{i(x_{mn}\Delta k_x + y_{mn}\Delta k_y)},$$

the maximum SHI enhancement by phase modulation can be expressed as:

$$\eta = \frac{I_{2\omega}(\varphi_n)_{max}}{I_{2\omega}(\varphi_n = 0)} = \frac{\left|\sum_{n=1}^{N} t_n e^{i2\varphi_n}\right|_{max}^2}{\left|\sum_{n=1}^{N} t_n\right|^2} = \frac{(\sum_{n=1}^{N}|t_n|)^2}{\left|\sum_{n=1}^{N} t_n\right|^2} \qquad (4.8)$$

Now, we consider the average values $<\eta>$ over a statistically significant number of structures with randomly distributed domain sizes, polarizations and positions. In general, the phase of t_n takes any value between 0 and 2π with equal probability. Consequently, the average maximum SHI enhancement by phase modulation is $\eta = 1 + \pi (N-1)/4$ (Figure 4.13). Note that this expression for η is in fact equal to the phase modulation enhancement through turbid linear media [107].

However, for the SHG in the Cerenkov and the collinear angle, the contribution from the structure boundaries (I_{bulk}) that behaves like in the homogeneous crystal, can be relatively large compared with the contribution from the random structure (I_{random}). In the collinear angle, the average enhancement in the collinear angle can take values $1 \leq \eta \leq 1+\pi (N-1)/4$, while the smallest value is due to the bulk boundary effect, and the biggest value is due to the disorder effect (Figure 4.13). In the Cerenkov angle, the average enhancement in the Cerenkov angle could take values between $1+\pi (N-1)/4 \leq \eta \leq N^2/\left|\sum_{n=1}^{N} e^{inL\Delta k_y}\right|^2$, while the smallest value is due to the disorder effect, and the biggest value is due to the bulk boundary effect. If the phase modulated segments are chosen with the appropriate width, the effect of the crystal boundaries makes the average enhancement in the Cerenkov angle to be substantially larger than at other angles (Figure 4.13b). Note also in the example given in Figure 4.13a the oscillation in $<\eta>$ produced by a segment width $L < \pi/\Delta k_y$ as explained in Section 4.3.1.

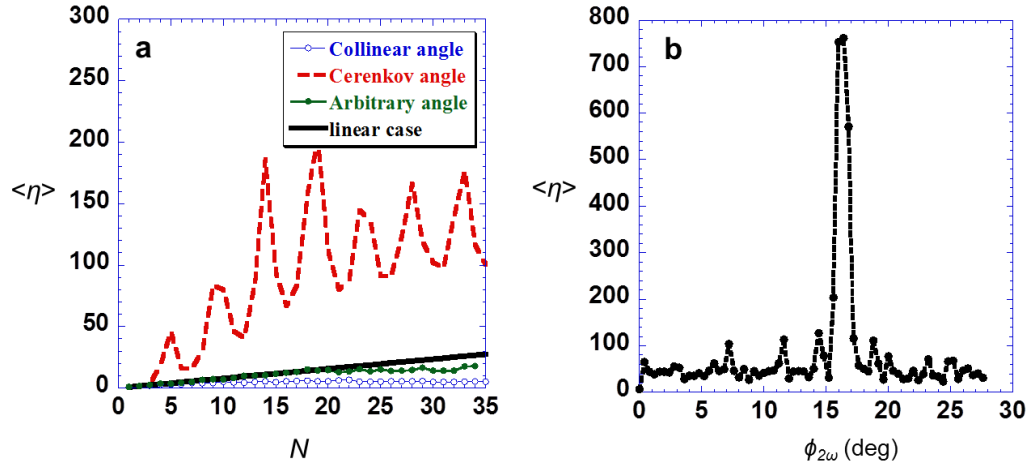

Figure 4.13: (a) Maximum SHI enhancement efficiency as a function of the phase segment number N, at an arbitrary angle $\phi_{2\omega}$ = 30°, collinear angle $\phi_{2\omega}$ = 0° and Cerenkov angle $\phi_{2\omega}$ = 16.8°. The black solid line corresponds to the linear enhancement efficiency $1+\pi$ (N-1)/4. The structure is 3N μm wide and 30 μm long, including domains with random sizes between 0 and 3 μm and random polarization. Each plot corresponds to the average over 100 different realizations of the randomness. (b) The maximum SHI enhancement efficiency as a function of the target direction from the same structure when N=50.

It is worth to conclude that, in either collinear or Cerenkov direction, a larger crystal width L_y results in a smaller η, closer to the minimum value in their individual efficiency ranges. This is due to the boundary effect in the collinear direction and to the disorder effect in the Cerenkov direction, respectively. In the collinear direction under the plane wave input, I_{bulk} is proportional to L_y^2 (Figure 2.3d), while I_{random} is proportional to L_y (Figure 4.9a), so the wider the crystal is, the larger boundary effect, which gives the smaller η closer to 1. In the Cerenkov direction under the plane wave input, I_{bulk} oscillates with L_y (Figure 2.3f), while I_{random} is proportional to L_y (Figure 4.9b), so the wider the

crystal is, the larger random effect, which gives the smaller η closer to $1+\pi(N-1)/4$.

On the other hand, in either collinear or Cerenkov direction, a larger crystal length results in a larger η, closer to the maximum value in their individual efficiency ranges. In that case due to the disorder effect in collinear direction and to the boundary effect in the Cerenkov direction. In the Cerenkov direction under the plane wave input, I_{bulk} is proportional to L_x^2 (Figure 2.3e), while I_{random} is proportional to L_x (Figure 4.8b), so the longer the crystal is, the larger boundary effect, which gives the larger η closer to $N^2/\left|\sum_{n=1}^{N} e^{inL\Delta k_y}\right|^2$. In the collinear direction under the plane wave input, I_{bulk} oscillates with L_x (Figure 2.3c), while I_{random} is proportional to L_x (Figure 4.8a), so the longer the crystal is, the larger random effect, which gives the larger η closer to $1+\pi(N-1)/4$.

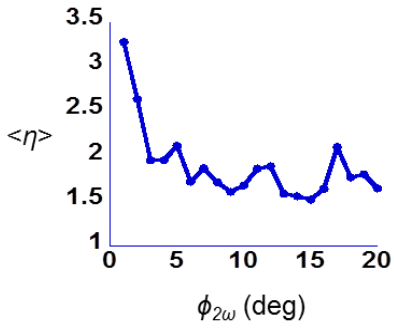

Figure 4.14: The SHI enhancement η decreases with the SHI optimization area angle from 0 to ϕ2ω. The structure width is 9 μm, and is composed of 3 phase groups of domains with random sizes between 0 and 3 μm, and half domains at random positions have opposite polarization (σ=1/2). The plot is the average of 10 random structures.

If we focus the SHI speckle from a random nonlinear structure (with uniform or random square domain size and randomly distributed opposite polarization) in one area, instead of only in one direction, the optimized SHI integration in that area will grow differently depending on whether the area range includes the Cerenkov angle for which $\Delta k_x=0$ and the collinear angle for which $\Delta k_y=0$. If it does not include the Cerenkov angle or the collinear angle, the SHG speckle size and number in that area does not change, the SHI integration in that area under plane wave input is proportional to MN, the optimized SHI integration in that area is proportional to MN^2, and the SHI enhancement will be $\eta=N$. If the area includes the Cerenkov angle or the collinear angle, and the SHG speckle size and number in that area does not change, the SHI integration in that area under plane wave input is proportional to $[(k\text{-}2)MN + MN^2+M^2\left|\sum_{n=1}^{N} e^{inL_{mn}\Delta k_y}\right|^2]$/k, where k is the total SHG speckle number in the SHG optimization area, L_{mn} randomly vary from 0 to L, and Δk_y is for the Cerenkov angle, and the optimized SHI integration in that area will be proportional to the value $[(k\text{-}1)MN^2+M^2N^2]/k$, and the SHI enhancement η takes the proportion of the optimized SHI and the SHI under plane wave input.

However, the demonstration above is the ideal case when the optimized area is small enough, so the phase modulation optimization conditions for all the speckles in that area are met. In practice, since the phase modulation can not satisfy the maximum SHG optimization conditions in different directions simultaneously, the bigger the optimized SHG

area is, the harder to optimize the SHG integration in that area, and the smaller η (Figure 4.14). Besides, as the number of square domains increases, the SHG speckle size decreases, with more speckles appearing, so the optimization of SHG in one area has a more complicated relation with the structure length and width.

4.4 Conclusions

The SHG diffusion in the c-plane highly limits its efficiency in one direction. We have experimentally implemented a wave-front phase modulation method to focus the SHG from an SBN crystal from many speckles to a single point. The experimental method shown for a transparent crystal is also completely generalizable to diffusive materials with changes in the refractive index producing multiple scattering.

In order to understand the experimental second order light generation optimization from the random nonlinear transparent SBN crystal, we present a 2D theory of the spatial intensity optimization of SHG by fundamental beam phase modulation. We demonstrate the different optimization efficiency and behavior of the SHG in different special angles, including the collinear SHG along the fundamental beam direction, the Cerenkov SHG in the transverse direction, and the SHG in an arbitrary representative direction.

Our theoretical calculations show that, in general, the SHI enhancement efficiency is equal to the one that can be obtained in linear diffusive media. However, in the collinear and the Cerenkov directions, the SHI can have an important contribution from the crystal boundaries. When the disorder in the bulk is present, such contribution can increase the maximum possible enhancement efficiency in the collinear direction, while it decreases that in the Cerenkov direction. When a wave-front phase modulation is included, in the collinear direction the SHI enhancement efficiency is within the limit of the one obtained in linear diffusive media, whereas at the Cerenkov angle, the enhancement efficiency brought by the phase modulation can lead to larger SHI.

Chapter 5

Conclusion

In the thesis we study theoretically and experimentally the propagation, generation and controlled manipulation of nonlinear light in random structures. The second harmonic light generation from random media is treated by solving the wave equation using the Green function formalism. First, SHG from one single nonlinear domain is obtained. Then, the SHG from the whole structure, composed of randomly distributed domains with different sizes, is simulated as the sum of the SHG from all the domains. With this theoretical model we predicted several characteristics of the nonlinear light generation which were not easily understood when using earlier models based on the random phase-matching condition, satisfied by a large number of k-vectors in varied directions.

The theoretical model is used to explain all the features of the experimentally observed nonlinear speckle generation from a transparent random structure. Indeed, the model can be applied to simulate the speckle generated from a structure where the randomness is in the nonlinear susceptibility but not in the linear part. The detailed SHG spatial distribution pattern is acquired through this model, and the simulated SHG shows a very good agreement with the experimental result.

In a second part of the thesis, a wavefront phase modulation scheme is developed to control such nonlinear light generation in random media. The results presented demonstrate experimentally a control of SHG through a random nonlinear crystal. We show that the SHG focus obtained by the phase modulation is about 700 times brighter than the SHG before optimization, which is about the same efficiency reached when controlling linear light through random media by the wavefront phase modulation method. On the other hand, the work also presents, theoretically, that in the collinear and Cerenkov directions, the uniform structure boundary contributes to a concentration behavior of the SHG, which can be distinguished from the random effect. In this way, it is demonstrated that, with the presence of a uniform structure boundary, without modifying the random structure, it is possible to get a much higher SHG concentration efficiency in the Cerenkov direction than in any other direction.

The analysis presented in this work expands the current understanding of nonlinear light control in complex media, and may contribute to the

development of a new class of imaging and focusing techniques based on nonlinear frequency mixing in random optical materials. On the basis of this thesis, further research can be carried out, as for instance, in the control of other types of nonlinear light generation, such as the difference frequency generation. Other methods to control the nonlinear light generation from random structures could be developed to improve the data acquisition speed. Other types of random structures, such as $LiNbO_3$ could also be studied.

Bibliography

[1] M. I. Mishchenko, L. D. Travis, and A. A. Lacis, Multiple scattering of light by particles. Cambridge, 2006.

[2] P. E. Wolf and G. Maret, “Weak Localization and Coherent Backscattering of Photons in Disordered Media,” Physical Review Letters, vol. 55, no. 24, pp. 2696–2699, 1985.

[3] E. Akkermans, P. E. Wolf, R. Maynard, and G. Maret, “Theoretical study of the coherent backscattering of light by disordered media,” J. Phys. France, vol. 49, pp. 77–98, 1988.

[4] K. M. Yoo, G. C. Tang, and R. R. Alfano, “Coherent backscattering of light from biological tissues.,” Applied optics, vol. 29, no. 22, pp. 3237–9, Aug. 1990.

[5] M. I. Mishchenko, “Diffuse and coherent backscattering by discrete random media—I. Radar reflectivity, polarization ratios, and enhancement factors for a half-space of polydisperse, nonabsorbing and absorbing spherical particles,” Journal of Quantitative Spectroscopy and Radiative Transfer, vol. 56, no. 5, pp. 673–702, Nov. 1996.

[6] V. P. Tishkovets and M. I. Mishchenko, “Coherent backscattering of light by a layer of discrete random medium,” Journal of Quantitative Spectroscopy and Radiative Transfer, vol. 86, no. 2, pp. 161–180, Jun. 2004.

[7] V. P. Tishkovets and M. I. Mishchenko, “Approximate calculation of coherent backscattering for semi-infinite discrete random media,” Journal of Quantitative Spectroscopy and Radiative Transfer, vol. 110, no. 1–2, pp. 139–145, Jan. 2009.

[8] O. Muskens, a. Koenderink, and W. Vos, “Broadband coherent backscattering spectroscopy of the interplay between order and disorder in three-dimensional opal photonic crystals,” Physical Review B, vol. 83, no. 15, pp. 155101, Apr. 2011.

[9] Y. A. Ilyushin, “Coherent backscattering enhancement in highly anisotropically scattering media: Numerical solution,” Journal of Quantitative Spectroscopy and Radiative Transfer, vol. 113, no. 5, pp. 348–354, Mar. 2012.

[10] C. López, “Anderson localization of light: A little disorder is just right,” Nature Physics, vol. 4, pp. 755–756, 2008.

[11] N. M. Lawandy, R. M. Balachandran, A. S. L. Gomes, and E. Sauvain, "Laser action in strongly scattering media," Nature, vol. 368, pp. 436–438, 1994.

[12] R. M. Balachandran, N. M. Lawandy, and J. a Moon, "Theory of laser action in scattering gain media," Optics letters, vol. 22, no. 5, pp. 319–321, Mar. 1997.

[13] H. Cao, Y. Zhao, S. Ho, E. Seelig, Q. Wang, and R. Chang, "Random laser action in semiconductor powder," Physical Review Letters, vol. 82, no. 11, pp. 2278–2281, Mar. 1999.

[14] D. Wiersma, "The smallest random laser," Nature, vol. 406, no. 6792, pp. 132–133, Jul. 2000.

[15] C. Vanneste, P. Sebbah, and H. Cao, "Lasing with resonant feedback in weakly scattering random systems," Physical Review Letters, vol. 98, no. 14, pp. 1–4, Apr. 2007.

[16] D. S. Wiersma, "The physics and applications of random lasers," Nature Physics, vol. 4, pp. 359–367, 2008.

[17] C. Conti and a. Fratalocchi, "Dynamic light diffusion, three-dimensional Anderson localization and lasing in inverted opals," Nature Physics, vol. 4, no. 10, pp. 794–798, Aug. 2008.

[18] J. Fallert, R. J. B. Dietz, J. Sartor, D. Schneider, C. Klingshirn, and H. Kalt, "Co-existence of strongly and weakly localized random laser modes," Nature Photonics, vol. 3, pp. 279–282, 2009.

[19] L. Yang, G. Feng, J. Yi, K. Yao, G. Deng, and S. Zhou, “Effective random laser action in Rhodamine 6G solution with Al nanoparticles,” Applied optics, vol. 50, no. 13, pp. 1816–1821, May 2011.

[20] D. Brogioli, A. Vailati and M. Giglio, 2002, “Heterodyne near-field scattering,” Applied Physics Letters, vol. 81, pp. 4109-4111, 2002.

[21] M. Francon, “Laser Speckle and Applications in Optics,” Academic press, INC., 1979.

[22] S. E. Murialdo, G. H. Sendra, L. I. Passoni, et al. “Analysis of bacterial chemotactic response using dynamic laser speckle,” Journal of biomedical optics, Vol.14, no. 6, pp. 4015-4016. 2009.

[23] Y. Zhao, J. L. Wang, X. P. Wu, F. W. Williams, R. J. Schmidt, “Point-wise and whole-field laser speckle intensity fluctuation measurements applied to botanical specimens,” Optics and Lasers in Engineering, Vol.28, Issue 6, pp. 443-456, 1997.

[24] R. A. Braga , I. M. Dal Fabbro , F. M. Borem, G. Rabelo, R. Arizaga, H. J. Rabal, M. Trivi, “Assessment of Seed Viability by Laser Speckle Techniques,” Biosystems Engineering, Vol. 86, Issue 3, pp. 287–294, 2003.

[25] S. L. Toh, C. Quan, K. C. Woo, C. J. Tay, H.M. Shang, “Whole field surface roughness measurement by laser speckle correlation technique,” Optics & Laser Technology, Vol. 33, Issue 6, pp. 427-434, 2001.

[26] P. A. Faccia, O. R. Pardini, J. I. Amalvy, N. Cap, E. E. Grumel, R. Arizaga, M. Trivi, "Differentiation of the drying time of paints by dynamic speckle interferometry," Progress in Organic Coating, Vol.64, Issue 4, pp.350-355, 2009.

[27] P. K. Rastogi, "Digital Speckle Pattern Interferometry and Related Techniques," Wiley, 2000.

[28] R. Jones, C. Wykes, "Holographic and speckle interferometry," Cambridge university press, 1989.

[29] J. I. Trisnadi, "Speckle contrast reduction in laser projection displays," Proceedings of SPIE, Vol. 4657, pp.131-137, 2002.

[30] K. V. Chellappan, E. Erden, and H. Urey, "Laser-based displays: a review," Applied Optics, Vol. 49, Issue 25, pp. F79-F98, 2010.

[31] T. Chaigne, O. Katz, A. C. Boccara, M. Fink, E. Bossy and S. Gigan, "Controlling light in scattering media non-invasively using the photoacoustic transmission matrix," Nature Photonics, Vol. 8, pp. 58-64, Nov. 2013.

[32] T. Bifano, "Adaptive imaging: MEMS deformable mirrors," Nature Photonics, Vol. 5, pp. 21-23, Jan. 2011.

[33] D. B. Conkey, A. M. Caravaca-Aguirre, and R. Piestun, "High-speed scattering medium characterization with application to focusing light through turbid media," Nature Photonics, Vol. 5, pp. 21-23, Jan. 2011.

[34] Z. Yaqoob, D. Psaltis, M. S. Feld, and C. Yang, “Optical Phase Conjugation for Turbidity Suppression in Biological Samples,” Nature photonics, vol. 2, no. 2, pp. 110–115, Jan. 2008.

[35] I. M. Vellekoop and a P. Mosk, “Focusing coherent light through opaque strongly scattering media.,” Optics letters, vol. 32, no. 16, pp. 2309–2311, Aug. 2007.

[36] G. Lerosey, J. de Rosny, A. Tourin, M. Fink, “Focusing Beyond the Diffraction Limit with Far-Field Time Reversal,” Science, vol. 315, no. 5815, pp. 1120–1122, Feb. 2007.

[37] R. W. Boyd, Nonlinear optics. Academic Press, 2008.

[38] P. A. Franken, A. E. Hill, C. W. Peters, and G. Weinreich, “Generation of optical harmonics,” Physical Review Letters, vol. 7, no. 4, pp. 118–119, 1961.

[39] S. Zhu, Y. Zhu, and N. Ming, “Quasi-Phase-Matched third-harmonic generation in a quasi-periodic optical superlattice,” Science, vol. 278, no. 5339, pp. 843–846, Oct. 1997.

[40] A. Bahabad, O. Cohen, M. M. Murnane, and H. C. Kapteyn, “Quasi-periodic and random quasi-phase-matching of high harmonic generation.,” Optics letters, vol. 33, no. 17, pp. 1936–8, Sep. 2008.

[41] M.Baudrier-Raybaut, R.haidar, Ph.Kupecek, Ph.Lemasson, and E.Rosencher, “Random quasi-phase-matching in bulk polycrystalline isotropic nonlinear materials,” Nature, vol. 432, pp. 374–376, 2004.

[42] R. Fischer, D. N. Neshev, S. M. Saltiel, A. a. Sukhorukov, W. Krolikowski, and Y. S. Kivshar, "Monitoring ultrashort pulses by transverse frequency doubling of counterpropagating pulses in random media," Applied Physics Letters, vol. 91, no. 3, pp. 031104, 2007.

[43] U. Voelker and K. Betzler, "Domain morphology from k-space spectroscopy of ferroelectric crystals," Physical Review B, vol. 74, no. 13, pp. 132104, Oct. 2006.

[44] X. Vidal and J. Martorell, "Generation of light in media with a random distribution of nonlinear domains," Physical Review Letters, vol. 97, no. 1, pp. 013902, Jul. 2006.

[45] F. J. Rodríguez, C. Yao, J. L. Domínguez-Juárez, J. Bravo-Abad, and J. Martorell, "Observation of speckle pattern formation in transparent nonlinear random media," Optics letters, vol. 36, no. 8, pp. 1347–1349, Apr. 2011.

[46] C. Yao, F. J. Rodríguez, and J. Martorell, "Controlling the diffused nonlinear light generated in random materials," Optics letters, vol. 37, no. 10, pp. 1676–1678, May 2012.

[47] M. M. Fejer, G. a. Magel, D. H. Jundt, and R. L. Byer, "Quasi-phase-matched second harmonic generation: tuning and tolerances," IEEE Journal of Quantum Electronics, vol. 28, no. 11, pp. 2631–2654, 1992.

[48] J. Bravo-abad, X. Vidal, J. L. Dom, and J. Martorell, "Optical second-harmonic scattering from a non-diffusive random distribution

of nonlinear domains," Optics express, vol. 18, no. 13, pp. 1167–1174, 2010.

[49] V. E. Kravtsov, V. M. Agranovich and K. I. Grigorishin, "Theory of second-harmonic generation in strongly scattering media," Physical Review B, Vol. 44, no. 10, pp.4931 , Sep. 1991.

[50] V. M. Shalaev, "Optical properties of nanostructured random media," Springer, 2002.

[51] V. Roppo, W.Wang, K. Kalinowski, Y. Kong, C. Cojocaru, J. Trull, R. Vilaseca, M. Scalora, W. Krolikowski, and Yu. Kivshar, "The role of ferroelectric domain structure in second harmonic generation in random quadratic media," Optics Express, vol. 18, no. 5, pp. 4012-4022, 2010.

[52] M. Ayoub, P. Roedig, J. Imbrock, and C. Denz, "Domain-shape-based modulation of Čerenkov second-harmonic generation in multidomain strontium barium niobate," Optics letters, vol. 36, no. 22, pp. 4371–4373, Nov. 2011.

[53] R. Fischer, S. M. Saltiel, D. N. Neshev, W. Krolikowski, and Y. S. Kivshar, "Broadband femtosecond frequency doubling in random media," Applied Physics Letters, vol. 89, no. 19, pp. 191105, 2006.

[54] K. A. Kuznetsov, G. K. Kitaeva, a. V. Shevlyuga, L. I. Ivleva, and T. R. Volk, "Second harmonic generation in a strontium barium niobate crystal with a random domain structure," JETP Letters, vol. 87, no. 2, pp. 98–102, Feb. 2011.

[55] Y. Sheng, J. Dou, B. Ma, B. Cheng, and D. Zhang, "Broadband efficient second harmonic generation in media with a short-range order," Applied Physics Letters, vol. 91, no. 1, pp. 011101, 2007.

[56] P. Molina, M. D. L. O. Ramírez, and L. E. Bausá, "Strontium Barium Niobate as a multifunctional two-dimensional nonlinear 'photonic glass'," Advanced Functional Materials, vol. 18, no. 5, pp. 709–715, Mar. 2008.

[57] V. V. Shvartsman, J. Dec, S. Miga, T. Łukasiewicz, and W. Kleemann, "Ferroelectric Domains in SrxBa1 −xNb2O6 Single Crystals ($0.4 \leq \times \leq 0.75$)," Ferroelectrics, vol. 376, no. 1–8, pp. 197–204, Dec. 2008.

[58] L. Tian, D. a. Scrymgeour, and V. Gopalan, "Real-time study of domain dynamics in ferroelectric Sr0.61Ba0.39Nb2O6," Journal of Applied Physics, vol. 97, no. 11, pp. 114111, 2005.

[59] U. Voelker, U. Heine, C. Gödecker, and K. Betzler, "Domain size effects in a uniaxial ferroelectric relaxor system: The case of SrxBa1−xNb2O6," Journal of Applied Physics, vol. 102, no. 11, pp. 114112, 2007.

[60] M. Ramírez, D. Jaque, L. Bausá, J. García Solé, and A. Kaminskii, "Coherent light generation from a Nd:SBN nonlinear laser crystal through its ferroelectric phase transition," Physical Review Letters, vol. 95, no. 26, pp. 267401, Dec. 2005.

[61] A. Tunyagi, M. Ulex, and K. Betzler, “Noncollinear optical frequency doubling in strontium barium niobate,” Physical Review Letters, vol. 90, no. 24, pp. 243901, Jun. 2003.

[62] K. Kalinowski, P. Roedig, Y. Sheng, M. Ayoub, J. Imbrock, C. Denz, and W. Krolikowski, “Enhanced Čerenkov second-harmonic emission in nonlinear photonic structures,” Optics letters, vol. 37, no. 11, pp. 1832–1834, Jun. 2012.

[63] S. M. Saltiel, Y. Sheng, N. Voloch-Bloch, D. N. Neshev, W. Krolikowski, A. Arie, K. Koynov, and Y. S. Kivshar, “Cerenkov-type second-harmonic generation in two-dimensional nonlinear photonic structures,” IEEE Journal of Quantum Electronics, vol. 45, no. 11, pp. 1465–1472, Nov. 2009.

[64] Y. Sheng, V. Roppo, M. Ren, K. Kalinowski, C. Cojocaru, J. Trull, Z. Li, K. Koynov, and W. Krolikowski, “Multi-directional Cerenkov second harmonic generation in two-dimensional nonlinear photonic crystal,” Optics express, vol. 20, no. 4, pp. 3948–3953, 2012.

[65] W. Wang, Y. Sheng, Y. Kong, A. Arie, and W. Krolikowski, “Multiple Čerenkov second-harmonic waves in a two-dimensional nonlinear photonic structure,” Optics letters, vol. 35, no. 22, pp. 3790–3792, Nov. 2010.

[66] P. D. Maker, R. W. Terhune, M. Nisenoff, and and C. M. Savage, “Effects of dispersion and focusing on the production of optical harmonics,” Physical Review Letters, vol. 8, no. 1, pp. 21–22, 1962.

[67] P. Pavlides and D. Pugh, “General theory of Maker fringes in crystals of low symmetry,” Journal of Physics: Condensed Matter, vol. 3, no. 8, pp. 967–988, Feb. 1991.

[68] P. B. Jamieson, “Ferroelectric tungsten bronze-type crystal structures. I. Barium Strontium Niobate Ba0.27Sr0.75Nb2O5.78,” The Journal of Chemical Physics, vol. 48, no. 11, pp. 5048–5057, 1968.

[69] A. M. Glass, “Investigation of the electrical properties of Sr1−xBaxNb2O6 with special reference to pyroelectric detection,” Journal of Applied Physics, vol. 40, no. 12, pp. 4699–4713, 1969.

[70] P. Lehnen, E. Beckers, W. Kleemann, T. Woike, and R. Pankrath, “Ferroelectric domains in the uniaxial relaxor system SBN:Ce, Cr and Co,” Ferroelectrics, vol. 253, no. 1, pp. 11–19, Feb. 2001.

[71] M. Goulkov, M. Imlau, T. Granzow, and T. Woike, “Beam fanning reversal in the ferroelectic relaxor Sr0.61Ba0.39Nb2O6 at high external electric fields,” Journal of Applied Physics, vol. 94, no. 8, pp. 4763–4771, 2003.

[72] T. Granzow, T. Woike, M. Wöhlecke, M. Imlau, and W. Kleemann, “Change from 3D-Ising to random field-Ising-model criticality in a uniaxial relaxor ferroelectric,” Physical Review Letters, vol. 92, no. 6, pp. 065701, Feb. 2004.

[73] P. Lehnen, W. Kleemann, T. Woike, and R. Pankrath, “Ferroelectric nanodomains in the uniaxial relaxor system Sr0.61-

xBa0.39Nb2O6:Cex3+," Physical Review B, vol. 64, no. 22, pp. 224109, Nov. 2001.

[74] A. I. Bezhanova, V. I. Silvestrov, T. A. Zeinalova, and T. R. Volk, "Domain dynamics of strontium-barium niobate crystals in low-frequency electric fields," Ferroelectrics, vol. 111, pp. 299–305, Nov. 1990.

[75] E. Soergel, "Visualization of ferroelectric domains in bulk single crystals," Applied Physics B, vol. 81, pp. 729–751, Oct. 2005.

[76] K. Nassau, H. J. Levinstein, and G. M. Loiacono, "The domain structure and etching of ferroelectric Lithium Niobate," Applied Physics Letters, vol. 6, no. 11, pp. 228–229, 1965.

[77] M. Ayoub, J. Imbrock, and C. Denz, "Second harmonic generation in multi-domain $\chi 2$ media: from disorder to order.," Optics express, vol. 19, no. 12, pp. 11340–11354, Jun. 2011.

[78] S. Kurimura and Y. Uesu, "Application of the second harmonic generation microscope to nondestructive observation of periodically poled ferroelectric domains in quasi-phase-matched wavelength converters," Journal of Applied Physics, vol. 81, no. 1, pp. 369–375, 1997.

[79] Y. Uesu, S. Kurimura, and Y. Yamamoto, "Optical second harmonic images of 90° domain structure in BaTiO3 and periodically inverted antiparallel domains in LiTaO3," Applied Physics Letters, vol. 66, no. 17, pp. 2165, 1995.

[80] K. Terabe, S. Takekawa, M. Nakamura, K. Kitamura, S. Higuchi, Y. Gotoh, and A. Gruverman, "Imaging and engineering the nanoscale-domain structure of a Sr0.61Ba0.39Nb2O6 crystal using a scanning force microscope," Applied Physics Letters, vol. 81, no. 11, pp. 2044–2046, 2002.

[81] Y. Sheng, A. Best, H.-J. Butt, W. Krolikowski, A. Arie, and K. Koynov, "Three-dimensional ferroelectric domain visualization by Cerenkov-type second harmonic generation," Optics express, vol. 18, no. 16, pp. 16539–16545, 2010.

[82] A. R. Tunyagi, "Non-Collinear second harmonic generation in strontium barium niobate," 2004.

[83] M. Horowitz, A. Bekker, and B. Fischer, "Simultaneous generation of sum , difference , and harmonics frequencies by spread spectrum phase-matching," Applied Physics Letters, vol. 65, no. 6, pp. 679–681, 1994.

[84] S. Wang, V. Pasiskevicius, and F. Laurell, "Dynamics of green light-induced infrared absorption in KTiOPO4 and periodically poled KTiOPO4," Journal of Applied Physics, vol. 96, no. 4, pp. 2023–2028, 2004.

[85] S. Orlov, M. Segev, A. Yariv, and R. R. Neurgaonkar, "Light-induced absorption in photorefractive strontium barium niobate," Optics letters, vol. 19, no. 17, pp. 1293–1295, Sep. 1994.

[86] S. Kawai, T. Ogawa, H. S. Lee, R. C. Dematteі, and R. S. Feigelson, “SHG from needlelike ferroelectric domains in SBN single crystals,” Applied Physics Letters, vol. 73, no. 6, pp. 768–770, 1998.

[87] J. W. Goodman, “Some fundamental properties of speckle*,” Journal of the Optical Society of America, vol. 66, no. 11, pp. 1145–1150, 1976.

[88] J.C. Dainty, Laser speckle and related phenomena, vol. 1. 1975.

[89] J. W. Goodman, Speckle phenomena in optics: Theory and applications, vol. 130, no. 2. Roberts and Company Publishers, 2007.

[90] R. Carminati, “Subwavelength spatial correlations in near-field speckle patterns,” Physical Review A, vol. 81, no. 5, pp. 053804, May 2010.

[91] N. A. Chang and N. George, “Speckle in the 4F optical system,” Applied optics, vol. 47, no. 4, pp. A13–20, Feb. 2008.

[92] S. Feng, “Correlations and fluctuations of coherent wave transmission through disordered media,” Physical Review Letters, vol. 61, no. 7, pp. 834–837, 1988.

[93] J. H. Li and A. Z. Genack, “Correlation in laser speckle,” Physical Review E, vol. 49, no. 5, pp. 4530–4533, 1994.

[94] Z. Wang, K. J. Webb, and A. M. Weiner, “Coherent incident field information through thick random scattering media from speckle

correlations over source position.," Applied optics, vol. 49, no. 30, pp. 5899–5905, Oct. 2010.

[95] B. Shapiro, "Large Intensity Fluctuations for wave Propagation in Random Media," Physical Review Letters, vol. 57, no. 17, pp. 2168–2171, 1986.

[96] I. Freund, M. Rosenbluh, and S. Feng, "Memory effects in propagation of optical waves through disordered media," Physical review letters, vol. 61, no. 20, pp. 2328–2331, Nov. 1988.

[97] M. Tomita, "Time-resolved fluctuations and the memory effect in disordered optical media," Physical Review B, vol. 45, no. 2, pp. 1045–1048, Dec. 1992.

[98] T. Ito and M. Tomita, "Speckle correlation measurement in a disordered medium observed through second-harmonics generation," Physical Review E, vol. 69, no. 3, pp. 036610, Mar. 2004.

[99] S. E. Skipetrov, "Dynamic instability of speckle patterns in nonlinear random media," Journal of the Optical Society of America B, vol. 21, no. 1, pp. 168–176, 2004.

[100] A. Derode, P. Roux, and M. Fink, "Robust acoustic time reversal with high-order multiple scattering," Physical Review Letters, vol. 75, no. 23, pp. 4206–4210, 1995.

[101] C. L. Hsieh, Y. Pu, R. Grange, and D. Psaltis, "Digital phase conjugation of second harmonic radiation emitted by nanoparticles in turbid media," Optics express, vol. 18, no. 12, pp. 12283–12290, 2010.

[102] C. L. Hsieh, Y. Pu, R. Grange, G. Laporte, and D. Psaltis, “Imaging through turbid layers by scanning the phase conjugated second harmonic radiation from a nanoparticle,” Optics express, vol. 18, no. 20, pp. 20723–20731, Sep. 2010.

[103] E. G. van Putten, and A. Mosk, “Viewpoint: The information age in optics: Measuring the transmission matrix,” Physics, vol. 3, pp. 22, Mar. 2010.

[104] M. Kim, Y. Choi, C. Yoon, W. Choi, J. Kim, Q. Park, and W. Choi, “Maximal energy transport through disordered media with the implementation of transmission eigenchannels,” Nature Photonics, vol. 6, pp. 583–587, 2012.

[105] S. M. Popoff, G. Lerosey, R. Carminati, M. Fink, a. C. Boccara, and S. Gigan, “Measuring the transmission matrix in optics: An approach to the study and control of light propagation in disordered media,” Physical Review Letters, vol. 104, no. 10, pp. 100601, Mar. 2010.

[106] S. M. Popoff, G. Lerosey, M. Fink, a C. Boccara, and S. Gigan, “Controlling light through optical disordered media: transmission matrix approach,” New Journal of Physics, vol. 13, no. 12, pp. 123021, Dec. 2011.

[107] I. M. Vellekoop and a. P. Mosk, “Phase control algorithms for focusing light through turbid media,” Optics Communications, vol. 281, no. 11, pp. 3071–3080, Jun. 2008.

[108] Tomás Cizmár, M. Mazilu, and K. Dholakia, "In situ wave-front correction and its application to micromanipulation," Nature Photonics, vol. 4, pp. 388–394, 2010.

[109] A. M. Weiner, "Ultrafast optics: Focusing through scattering media," Nature Photonics, vol. 5, pp. 332–334, 2011.

[110] I. M. Vellekoop, a. Lagendijk, and a. P. Mosk, "Exploiting disorder for perfect focusing," Nature Photonics, vol. 4, no. 5, pp. 320–322, Feb. 2010.

[111] E. G. van Putten, D. Akbulut, J. Bertolotti, W. L. Vos, A. Lagendijk, and a P. Mosk, "Scattering lens resolves sub-100 nm structures with visible light," Physical review letters, vol. 106, no. 19, pp. 193905, May 2011.

[112] O. Katz, E. Small, Y. Bromberg, and Y. Silberberg, "Focusing and compression of ultrashort pulses through scattering media," Nature Photonics, vol. 5, no. 6, pp. 372–377, May 2011.

[113] M. Fink, "Imaging: Sharper focus by random scattering," Nature Photonics, vol. 4, pp. 269–271, May 2010.

[114] M. Cui, "Parallel wave-front optimization method for focusing light through random scattering media.," Optics letters, vol. 36, no. 6, pp. 870–2, Mar. 2011.

[115] Y. Choi, T. Yang, C. Fang-Yen, P. Kang, K. Lee, R. Dasari, M. Feld, and W. Choi, "Overcoming the diffraction limit using multiple

light scattering in a highly disordered medium," Physical Review Letters, vol. 107, no. 2, pp. 023902, Jul. 2011.

[116] I. M. Vellekoop and A. Mosk, "Universal optimal transmission of light through disordered materials," Physical Review Letters, vol. 101, no. 12, pp. 120601, Sep. 2008.

[117] J. Pendry, "Light finds a way through the maze," Physics, vol. 1, no. 20, pp. 8–10, Sep. 2008.

[118] S. M. Popoff, G. Lerosey, M. Fink, A. C. Boccara, and S. Gigan, "Image Transmission Through an Opaque Material," Nature Communications, vol. 1, no. 81, pp. 1–7, 2010.

[119] O. Katz, E. Small, and Y. Silberberg, "Looking around corners and through thin turbid layers in real time with scattered incoherent light," Nature Photonics, vol. 6, pp. 549–553, 2012.

[120] E. J. McDowell, M. Cui, I. M. Vellekoop, V. Senekerimyan, Z. Yaqoob, and C. Yang, "Turbidity suppression from the ballistic to the diffusive regime in biological tissues using optical phase conjugation.," Journal of biomedical optics, vol. 15, no. 2, pp. 025004, 2010.

[121] N. Bachelard, J. Andreasen, S. Gigan, and P. Sebbah, "Taming random lasers through active spatial control of the pump," Physical Review Letters, vol. 109, no. 3, pp. 033903, Jul. 2012.

[122] J. A. Davis, J. Nicolás, and A. Márquez, "Phasor analysis of eigenvectors generated in liquid-crystal displays," Applied optics, vol. 41, no. 22, pp. 4579–4584, 2002.

[123] E. G. van Putten, I. M. Vellekoop, and a P. Mosk, "Spatial amplitude and phase modulation using commercial twisted nematic LCDs," Applied optics, vol. 47, no. 12, pp. 2076–2081, Apr. 2008.

[124] I. M. Vellekoop, "Controlling the propagation of light in disordered scattering media," Doctoral thesis, 2008.

[125] J. J. Romero, D. Jaque, J. García Solé, and a. a. Kaminskii, "Simultaneous generation of coherent light in the three fundamental colors by quasicylindrical ferroelectric domains in Sr0.6 Ba0.4 (NbO3)2," Applied Physics Letters, vol. 81, no. 22, pp. 4106–4108, 2002.

** We applied the software Mathematica using the Nmaximize function with the DifferentialEvolution method to obtain the maximum SHG enhancement efficiency